

1 Implementing plant hydraulics in the Community Land Model

2 **Daniel Kennedy¹, Sean Swenson², Keith Oleson², David Lawrence², Rosie Fisher², Pierre
3 Gentine¹**

4 ¹Columbia

5 ²National Center for Atmospheric Research, Table Mesa Drive, Boulder, Colorado, USA

6 **Key Points:**

- 7 • A simplified soil-plant-atmosphere continuum model based on hydraulic theory is
8 implemented in the Community Land Model (version 5).
- 9 • Prognostic leaf water potential replaces soil matric potential as the functional basis
10 for water stress, thus reflecting how the leaf water supply (via the xylem network) and
11 evaporative demand act in concert to determine plant water status and thus stomatal
12 conductance and leaf gas exchange.
- 13 • Prognostic root water potential is used to implement hydraulic root water uptake, re-
14 placing the heuristic soil 'wilting' factor .

Abstract

= enter abstract here =

1 Introduction

Trees face emerging climate change risk globally [Allen *et al.*, 2010; Anderegg *et al.*, 2013a]. Understanding vegetation response is a high priority, both for discerning climate impacts and for modeling feedbacks to the carbon and hydrological cycles. In addition to stress from soil moisture drought, vegetation is susceptible to increasing atmospheric transpiration demand [Restaino *et al.*, 2016; Novick *et al.*, 2016a]. Increases in vapor pressure deficit (VPD) have occurred with warming [Ficklin and Novick, 2017; Seager *et al.*, 2015], and are associated with impacts on vegetation [Williams *et al.*, 2013; McDowell and Allen, 2015]. Significant uncertainty remains regarding how vegetation will respond to changes in hydroclimate within Earth System Models, feeding back onto the carbon cycle as vegetation mediates carbon uptake from continents [De Kauwe *et al.*, 2017; Friedlingstein *et al.*, 2014].

Plant water stress parameterizations are important in Earth System Models, as they define vegetation regulation of surface fluxes (photosynthesis, transpiration) to water fluctuations. Vegetation water use strategies also modulate carbon uptake, creating a critical coupling between the Earth System's carbon and hydrological cycles [Green *et al.*, 2017]. Drought stress parameterizations (functions which relate simple metric of soil moisture status to leaf gas exchange) are widely used to define the response of stomatal conductance to vegetation water status that is used to attenuate transpiration, photosynthesis, and root water uptake with drying. The dynamics of water stress in models have broad effects on critical land surface processes [?]. On diurnal timescales drought parameterizations influence the partitioning of latent versus sensible heat with effects on surface temperature [Bonan *et al.*, 2014]. On longer timescales vegetation water use strategies regulate the global carbon and water cycles [De Kauwe *et al.*, 2015].

Many recent studies have aimed at advancing the representation of water flow through the Soil-Plant-Atmosphere continuum (SPAC) in models [Xu *et al.*, 2016; Christoffersen *et al.*, 2016; Sperry *et al.*, 2017]. Modeling water flow through the SPAC adds complexity, but is in line with evidence of dynamic regulation of vegetation water use in response to both soil and atmospheric drying [Sperry and Love, 2015]. Furthermore, via Darcy's Law, SPAC models have a robust physical basis. Parameter estimation is challenging [Drake *et al.*, 2017], but hydraulic trait information is available [Kattge *et al.*, 2011; Anderegg, 2015a] and can be informative of forest vulnerability to drought [Choat *et al.*, 2012]. Likewise vegetation water status observations are available at a scale that is directly relevant to model development [Konings *et al.*, 2016; Grant *et al.*, 2016] and can be used to validate model results [Momen *et al.*, 2017; Konings *et al.*, 2017b].

Representation of vegetation water stress in the Community Land Model (CLM) and other land surface models is a known deficiency, with implications for the representation of the dry/wet season in tropical rainforests [Powell *et al.*, 2013; Ukkola *et al.*, 2016]. In this study, we update the CLM vegetation hydrodynamics parameterization based on hydraulic theory and analyze its dynamics using point simulations set within the Caxiuanã through-fall exclusion experiment [Fisher *et al.*, 2006]. Advancing the representation of the SPAC introduces a new state variable to CLM, vegetation water potential, which is valuable for modeling vegetation hydrodynamics. Modeling vegetation water potential allows for an explicit representation of water supply, from the soil through the vegetation substrate. This can incorporate a range of water use strategies and improves the model connection between allocation decisions and water availability. Root water uptake can be based on Darcy's law, in lieu of an empirical transpiration partitioning heuristic.

Vegetation water potential also improves the modeling of water demand. Transpiration is typically attenuated with drought stress according to vegetation water status, capturing

dynamic vegetation water use regulation. Leaf water potential serves as an improved metric for water status, in lieu of soil water or soil matric potential. This reflects vegetation sensitivity to both soil and atmospheric drying, while serving as a diagnostic for excessive xylem tension and cavitation risk. Modeling vegetation water potential also creates a framework for representing hydraulic redistribution [Lee *et al.*, 2005] and connecting to remote sensing observations (e.g. Vegetation Optcal Depth) [?].

In this study, we developed a simplified plant hydraulic implementation within CLM5, which we refer to as the 'Plant Hydraulic Stress' (PHS) configuration. SAY IN WHICH SECTION WE WILL FINE EACH PART PHS creates a framework to represent vegetation water potential, which is used to improve model vegetation hydrodynamics. Leaf water potential replaces soil potential as the functional basis for drought stress attenuation of transpiration and photosynthesis. Root water potential is used to model gradient-based root water uptake in lieu of a soil wilting factor heuristic function.

To assess the new model formulation, we carried out point simulations at Caxiuanã National Forest in Brazil. This site features a critical biome (terra-firme moist tropical evergreen forest) subject to experimental through-fall exclusion, where we expect vegetation regulation of transpiration and photosynthesis. We compare PHS with the former CLM hydrodynamics configuration, analyzing the dynamics of modeled water stress and root water uptake.

2 Model Description

2.1 Photosynthesis

The CLM5 photosynthesis model is derived from the CLM4.5 as described in Bonan *et al.* [2011], Thornton and Zimmermann [2007], and Oleson *et al.* [2013]. Photosynthesis is defined in three regimes: Rubisco-limited, light-limited, and export-limited following Farquhar *et al.* [1980] and Harley *et al.* [1992]. The implementation extends Sellers *et al.* [1996a,b] with co-limitation following Collatz *et al.* [1991].

CLM5 photosynthesis, in its default configuration, is a two-big-leaf model, with a sunlit and shaded leaf for each plant functional type [Thornton and Zimmermann, 2007; Dai *et al.*, 2004; Oleson *et al.*, 2013]. The canopy fluxes module iterates the solution for leaf temperature to satisfy the leaf surface energy balance, while environmental conditions are evolving. Within this, the photosynthesis module further iterates to solve for inter-cellular CO₂ concentration, balancing stomatal flux of CO₂ with photosynthetic assimilation flux of CO₂.

2.2 Stomatal Conductance

CLM5 implements the Medlyn stomatal conductance model, which reconciles the empirical and optimal approaches to modeling stomatal conductance [Medlyn *et al.*, 2011]. Stomatal conductance of CO₂ is thus directly related to net photosynthesis (A_n), CO₂ concentration at the leaf surface (C_a), and the square root of the vapor pressure deficit near the leaf surface (\sqrt{D}).

$$g_s = g_0 + \left(1 + \frac{g_1}{\sqrt{D}} \right) \frac{A}{C_a} \quad (1)$$

The model features two parameters g_0 ($\mu\text{mol} / \text{m}^2 / \text{s}$) and g_1 ($\text{kPa}^{0.5}$). The g_0 parameter is minimum stomatal conductance, representing cuticular and epidermal losses (small). The g_1 parameter relates to the marginal water cost guiding the optimization of carbon assimilation. Those parameters are plant functional type dependent.

The Medlyn model, derived from stomatal optimization theory, predicts stomatal conductance to maximize assimilation relative to water costs ($A - \lambda E$), but does not resolve concurrent limitations to stomatal conductance associated with drought conditions. Much recent work has focused on alternative constraints on plant hydrodynamics, especially in response

111 to drying soils [Manzoni *et al.*, 2013a; Novick *et al.*, 2016b; Zhou *et al.*, 2014]. This includes
 112 how plants manage the risk of cavitation associated with increasing xylem tension [Sperry
 113 *et al.*, 1998]. Reflecting drought limitations on diffusive fluxes, land surface models typically
 114 include a water stress factor, with various approaches for where to apply stress.

115 These water stress factors (in our case, f_w), are used to represent stomatal and non-
 116 stomatal limitation not captured by the base stomatal conductance model. Uncertainty re-
 117 mains within the literature for how to apply water stress to photosynthesis and stomatal con-
 118 ductance. One line of reasoning eschews the optimization of $A - \lambda E$ in favor of hydraulic
 119 costs [Sperry *et al.*, 2017], Studies also explore soil water adjustments to the marginal water
 120 cost, implemented by adjusting λ or Medlyn g_1 based on soil water [Manzoni *et al.*, 2013a].
 121 However, this may underestimate drought effects on photosynthesis [Zhou *et al.*, 2013; Lin
 122 *et al.*, 2018]. Yet other groups take a hybrid approach, combining stomatal optimization,
 123 with hydraulic constraints and/or so-called non-stomatal limitation, with stress attenuating
 124 V_{cmax} or mesophyll conductance (both of which feed back through photosynthesis to lower
 125 stomatal conductance) [Egea *et al.*, 2011; Novick *et al.*, 2016b].

126 Vegetation water stress is implemented via the vegetation water stress factor (f_w , di-
 127 mensionless, 0 to 1, formerly β_t). There are many different approaches for how to apply
 128 stress [Zhou *et al.*, 2013; Novick *et al.*, 2016b; Sperry and Love, 2015]. In CLM, f_w multi-
 129 plies the rate of maximum carboxylation (V_{cmax}) as described in Oleson *et al.* [2013]. While
 130 many models opt for soil-moisture based stomatal limitation (linking the stomatal con-
 131 ductance model slope parameter to soil moisture), Lin *et al.* [2018] found that only g_0 was sen-
 132 sitive to soil moisture (and not g_1). Zhou *et al.* [2013] suggests that changes in assimilation
 133 tend to exceed those predicted by modulating g_1 with soil moisture, but could be captured
 134 by changing V_{cmax} . Some field studies suggest V_{cmax} is not changing with drought, whereby
 135 model V_{cmax} instead may implicitly account for mesophyll conductance changes [Flexas
 136 *et al.*, 2004].

137 We opt for a simplified form of this stress approach, which seems to be consistent with
 138 field observations [Lin *et al.*, 2018]. Prognostic water stress (f_w , ranging from 0-1) attenu-
 139 ates stomatal conductance indirectly via multiplication of V_{cmax} , rather than the full conduc-
 140 tance for instance (inconsistent with observations Lin *et al.* [2018]). Water stress then lowers
 141 assimilation, which is coupled to stomatal conductance (CITE MEDLYN CONDUCTANCE).

142 Water stress is modeled as a function of leaf water potential (see Section 2.3.3), with
 143 stress accumulating as leaf water potentials become more negative. This reflects a notion of
 144 hydraulic safety, with vegetation avoiding excessive xylem tension associated with risk of
 145 cavitation.

146 With PHS, f_w replaces the CLM4.5 transpiration beta function (β_t). These factors
 147 are used by the photosynthesis model in the same way, but calculated differently. The PHS
 148 parameterization for f_w is based on leaf water potential (see Section 2.3.3). Previously the
 149 parameterization was based on soil water potential (see Section 3). Utilizing leaf water po-
 150 tential adopts a framework where stomatal conductance optimized for carbon gain is con-
 151 currently limited by hydraulic constraints [Novick *et al.*, 2016b]. As a result, not only water
 152 (bottom-up) stress induces moisture stress but also increased VPD propagating a drying into
 153 the xylem (top down stress).

154 2.3 Plant Hydraulic Stress (PHS)

155 In this study, we implemented a simplified plant hydraulic framework into CLM5 to
 156 calculate root water uptake and water stress attenuation of photosynthesis and transpiration.
 157 Using hydraulic (Darcy's) law and a corresponding electrical circuit analogy (Figure 1), we
 158 model the flow of water through the SPAC.

The hydraulic framework is used to diagnose water stress associated with increasing xylem tension and to calculate the root water uptake in each of (in this case) 20 vertically discretized soil layers. The combined water supply and demand implementations governing vegetation hydrodynamics is called Plant Hydraulic Stress (PHS). On the demand side, PHS redefines f_w , the CLM water stress factor, utilizing leaf water potential as its indicator for plant water status in lieu of soil potential. On the supply side, PHS adopts Darcy's Law to model root water uptake, replacing a soil-wilting-factor heuristic. By modeling vegetation water potential, we advance the physical basis plant water use, improving the dynamics of turbulent fluxes and root water uptake in response to water stress.

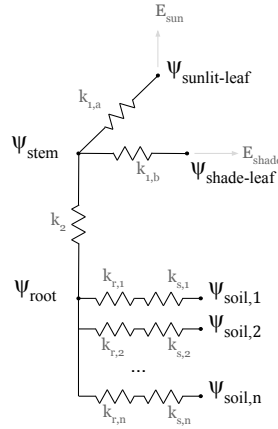


Figure 1. Plant hydraulic circuit analog schematic

2.3.1 Hydraulic schematic and segmentation

PHS solves for the set of SPAC vegetation water potential values ($\psi_{\text{root}}, \psi_{\text{stem}}, \psi_{\text{shade-leaf}}, \psi_{\text{sun-leaf}}$) that matches water supply (root water uptake) to water demand (transpiration), while maintaining continuity of water flow throughout the soil-plant-atmosphere continuum. Segmentation and other model design decisions followed a preference for a simplified implementation that, whenever possible, conformed to existing CLM model structure.

At each node in the circuit diagram, we model water potential, and, between nodes, we resolve the flux of water. The segmentation is designed to take advantage of field-measured hydraulic traits and to allow for differences in segment parameterizations [Simonin *et al.*, 2015; Sperry and Love, 2015]. Following from CLM, we utilize vertically discretized soil layers and a two-layer (sunlit vs. shaded) canopy. Soil layers are assumed to operate in parallel, which is a typical assumption justified by higher resistance in lateral versus central roots. Based on Darcy's law, we additionally segment the resistance across the soil matrix from the resistance through the root tissue [Williams *et al.*, 1996]. Specifics on the parameterization of conductance for each segment are provided in Appendix B.1.

2.3.2 Water supply

Water supply is modeled via Darcy's Law, where flow is proportional to the gradient in water potential. Flow of water (q) is the product of the path hydraulic conductance (k) and the gradient in water potential (accounting for changes in gravitational potential). Equation 2 represents the flow from a generic node 1 to node 2.

$$q = -k (\psi_2 - \psi_1 - \rho g \Delta z) \quad (2)$$

190 PHS does not represent plant tissue water storage (i.e., by circuit analogy the capacitance). Capacitance significantly complicates the water potential solution [Celia *et al.*, 1990]
 191 and is challenging to parameterize [Bartlett *et al.*, 2016]. However, buffering of water stress
 192 provided by tissue water storage could potentially be important especially on sub-daily timescales
 193 [Meinzer *et al.*, 2009; Epila *et al.*, 2017], whereby its inclusion may be warranted in future
 194 model generations.
 195

196 Vegetation segment conductance is modeled following empirical xylem vulnerability
 197 curves [Tyree and Sperry, 1989], where segments lose conductance with increasing xylem
 198 tension related to cavitation and embolism [Holbrook *et al.*, 2001]. The vulnerability curves
 199 model loss of conductance relative to maximum conductance using two parameters: c_k , a
 200 sigmoidal shape-fitting parameter, and p_{50} , the water potential at 50% loss of segment con-
 201 ductance (following Gentine *et al.* [2016]). These parameters can be estimated from field
 202 experiments [Sack *et al.*, 2002], and p_{50} is available in the TRY trait database [Kattge *et al.*,
 203 2011]. Parameterization based on p_{50} aligns with the call for a transition to a trait-based
 204 model paradigm [Anderegg, 2015a]. The loss of xylem conductivity is based on lower ter-
 205 minal water potential (ψ_1) as is typical in other simplified models [Xu *et al.*, 2016], but may
 206 underestimate the integrated loss of conductivity [Sperry and Love, 2015].

$$k = k_{\max} 2^{-\left(\frac{\psi_1}{p_{50}}\right)^{c_k}} \quad (3)$$

208 PHS models root, stem, and leaf tissue conductances according to equation 3. The pa-
 209 rameterization of k_{\max} varies by hydraulic segment (see details in Appendix B1). The con-
 210 ductance across the soil matrix to the root surface follows Williams *et al.* [2001] and Bonan
 211 *et al.* [2014] to estimate a characteristic distance between roots for the length-scaling of soil
 212 conductivity. Bulk soil resistivity is based on Clapp and Hornberger [1978] as described in
 213 Oleson *et al.* [2013]. Further details are provided in Appendix B1.

214 2.3.3 Water demand

215 Vegetation water demand and stomatal regulation is based on the Medlyn stomatal con-
 216 ductance model (see Section 2.2), which we adjust for water stress with f_w , the CLM water
 217 stress factor. As discussed earlier, the water stress factor multiplies V_{cmax} , which attenuating
 218 photosynthesis, which feeds back to lower stomatal conductance and transpiration. We cal-
 219 culate the water stress factor based on leaf water potential [Klein and Niu, 2014]. This is an
 220 update to CLM4.5, which bases f_w on soil water potential [Oleson *et al.*, 2013]. However,
 221 once calculated, f_w is deployed in the same way across versions of CLM (multiplies V_{cmax}).

222 As leaf water potential declines (because of transpiration) and xylem tension increases,
 223 transpiration is attenuated relative to its maximal value. The maximum transpiration ($E_{\text{sun,max}}$,
 224 $E_{\text{shade,max}}$) is defined as the value that resulting from Medlyn stomatal conductance absent
 225 water stress (achieved by setting $f_w = 1$). The fraction of maximum transpiration is mod-
 226 eled with a two-parameter sigmoidal function (Equation 4). The parameters are ψ_{50} , the leaf
 227 water potential at 50% loss of transpiration and c_k a sigmoidal shape-fitting parameter.

$$E_{\text{sun}} = E_{\text{sun,max}} 2^{-\left(\frac{\psi_{\text{sun-leaf}}}{\psi_{50}}\right)^{c_k}} \quad (4)$$

$$E_{\text{shade}} = E_{\text{shade,max}} 2^{-\left(\frac{\psi_{\text{shade-leaf}}}{\psi_{50}}\right)^{c_k}}$$

229 The value of f_w is based on the solution for attenuated transpiration (CLARIFY). We
 230 define f_w as the ratio of attenuated to maximal stomatal conductance (Equation 5). Maxi-
 231 mum stomatal conductance ($g_{s,\text{sun,max}}$, $g_{s,\text{shade,max}}$) is computed as the stomatal conductance

232 in the absence of water stress, i.e. $f_w = 1$. The attenuated stomatal conductance ($g_{s,sun}$,
 233 $g_{s,shade}$) is then the stomatal conductance associated with the PHS module water flow solution,
 234 which matches vegetation water supply with vegetation water demand (Section 2.3.4).

$$\begin{aligned} f_{w,sun} &= \frac{g_{s,sun}}{g_{s,sun,max}} \\ f_{w,shade} &= \frac{g_{s,shade}}{g_{s,shade,max}} \end{aligned} \quad (5)$$

236 Whereas the water supply parameters (see Section 2.3.2) relate to hydraulic traits often
 237 measured in the field, the hydraulic demand parameters ψ_{50} and c_k reflect the emergent
 238 property of hydraulic limitations to transpiration and must be empirically derived (WHAT
 239 ABOUT PLC CURVES?). Similarly, CLM4.5 features two empirical stomatal control pa-
 240 rameters, which are the soil matric potentials corresponding to stomates fully closed and sto-
 241 mates fully open (see Section 3). The representation of stomatal regulation with water stress
 242 is not generally agreed upon, and as such, should be investigated further. Recent modeling
 243 studies have proposed different forms [Sperry *et al.*, 2017; Xu *et al.*, 2016; Christoffersen
 244 *et al.*, 2016].

245 2.3.4 PHS solution

246 PHS solves for the set of vegetation water potential values (ψ) that matches water sup-
 247 ply (root water uptake) to water demand (transpiration), while satisfying continuity across
 248 the four water flow segments (soil-to-root, root-to-stem, stem-to-leaf, and leaves-to-transpiration).
 249 At each time step, we compute the flux divergence f (representing the mismatch of flow in
 250 and out of each segment) for a given set of vegetation water potential values ψ_i , and itera-
 251 tively update ψ until convergence is reached in terms of divergence, $f \rightarrow 0$.

$$\psi = \begin{bmatrix} \psi_{sun} \\ \psi_{shade} \\ \psi_{stem} \\ \psi_{root} \end{bmatrix} \quad (6)$$

$$f(\psi) = \begin{bmatrix} E_{sun} - q_{sun} \\ E_{shade} - q_{shade} \\ q_{sun} + q_{shade} - q_{stem} \\ q_{stem} - \sum_{j=1}^n q_{root,j} \end{bmatrix} \quad (7)$$

$$A = \frac{df}{d\psi} \quad (8)$$

255 While $|f| > 0$

$$\begin{aligned} \Delta\psi &= A^{-1} f(\psi_i) \\ \psi_{i+1} &= \psi_i + \Delta\psi \end{aligned} \quad (9)$$

257 The numerics are tractable because f has analytical derivatives and A (a 4x4 matrix
 258 with six null entries) is easy to invert when well-conditioned. Supply and demand converge,
 259 because transpiration demand decreases with more negative leaf water potentials and sup-
 260 ply increases with more negative leaf water potentials. Within a set of PHS iterations (9),
 261 transpiration is assumed to be linear with f_w . The PHS loop is nested within iterations for
 262 intercellular CO₂ concentration and leaf temperature. The non-linear relationship between
 263 f_w and transpiration is resolved through iteration for converging f_w alongside intercellular
 264 CO₂. Details on the numerical implementation are provided in Appendix Section B.1.

265 3 Water stress factor, SMS vs. PHS

266 PHS alters the transpiration beta function (β_t , colloquially BTRAN), SAY WAHT
 267 IT IS which is the phenomenological soil water stress function in CLM2-CLM4.5, as de-
 268 scribed in *Oleson et al.* [2013]. Because the name β_t is associated with this specific plant
 269 hydrodynamics representation, we opt to rename the variable to the water stress factor f_w .
 270 Throughout this paper we refer to the CLM4.5 plant hydrodynamics framework as SMS (soil
 271 moisture stress), as compared to the newer implementation, PHS (plant hydraulic stress). We
 272 adopt this terminology (in lieu of CLM4.5 vs. CLM5), because SMS is still deployable with
 273 CLM5.

274 With PHS, we interpret f_w as a drought safety mechanism, attenuating stomatal con-
 275 ductance to avoid excessive xylem tension associated with very negative leaf water potential.
 276 As such, f_w is parameterized as a function of prognostic leaf water potential. With SMS, f_w
 277 was calculated based on soil matric potential, as a root-fraction weighted average potential
 278 departure from an empirical soil layer wilting factor (Equation 10). In both parameteriza-
 279 tions, f_w multiplies V_{cmax} , attenuating photosynthesis and transpiration with drought. Re-
 280 cent studies suggest that the SMS parameterization introduces model bias in turbulent fluxes
 281 [Bonan et al., 2014] and contributes to unrealistic drought response of photosynthesis and
 282 stomatal conductance [Powell et al., 2013].

283 Such parameterizations (WHICH ONES?) have primarily been examined with appli-
 284 cation to stomatal conductance, but they are also used to define vegetation soil water extrac-
 285 tion. Each timestep, the transpiration flux solution must be distributed among the vertically
 286 discretized soil layers. In the SMS framework, the transpiration sink is partitioned by layer
 287 according to the soil layer wilting factor and root fraction. This framework lacks several key
 288 physical attributes of soil water extraction, which are addressed in the PHS implementation.
 289 In this section we present the SMS version of f_w and outline the differences as compared to
 290 PHS.

291 In SMS, the variable f_w is unitless, ranging from 0 to 1, with 1 corresponding to no
 292 water stress, and 0 corresponding to fully water stressed. It is calculated based on a root-
 293 fraction weighted average of soil layer wilting factor (w_i), which is a bounded linear function
 294 of soil water potential (ψ_i) relative to PFT parameters defining the soil potential with stom-
 295 ates fully open (ψ_o) and fully closed (ψ_c), among the soil layers $i = 1, \dots, n$. Note that root
 296 fraction (r_i) sums to 1, by definition.

$$297 f_w = \sum_{i=1}^n r_i w_i \quad (10)$$

$$298 w_i = 0 \leq \frac{\psi_i - \psi_c}{\psi_o - \psi_c} \leq 1 \quad (11)$$

299 In both stress parameterizations, f_w multiplies V_{cmax} to attenuate photosynthesis and
 300 stomatal conductance with soil water stress. With SMS, it is also directly used for modeling
 301 vegetation water extraction from the soil column. The total transpiration (T) is partitioned
 302 among the soil layers based on the f_w wilting factor. Within each soil layer, the contribution
 303 to total transpiration (q_i) depends on the layer root fraction and wilting factor, normalized by
 304 f_w :

$$305 q_i = \frac{r_i w_i}{f_w} T \quad (12)$$

306 Contrary to the heuristic SMS parameterization, the PHS implementation adopts a
 307 physically-based hydraulic framework, where the root water uptake (q_i) is the product of the
 308 hydraulic conductance (k_i) and the gradient in water potential ($-\Delta\psi$) driving the flow, i.e.
 309 obeying Darcy's law. That gradient is the difference between the root water potential (ψ_{root})

310 and the layer soil water potential (ψ_i), minus changes in gravitational potential, following
 311 Darcy's law.

312

$$\begin{aligned} q_i &= -k_i \Delta\psi \\ \Delta\psi &= (\psi_{\text{root}} - \psi_i - \rho g \Delta z) \end{aligned} \quad (13)$$

313 For comparison between SMS and PHS, we recast (12) into the hydraulic framework:
 314 defining T_{\max} , such that: $T = f_w T_{\max}$ to replace T in (12), and replacing w_i in (12) with the
 315 formula from (11).

316

$$q_i = \frac{T_{\max}}{\psi_o - \psi_c} r_i (\psi_i - \psi_c) \quad (14)$$

317 This yields SMS analogs for the hydraulic conductance and gradient terms of Equation
 318 13.

319

$$\begin{aligned} k_i &= r_i \frac{T_{\max}}{\psi_o - \psi_c} \\ \Delta\psi &= \psi_c - \psi_i \\ \text{constrained by: } \Delta\psi &= \begin{cases} 0 & \text{if } \psi_i < \psi_c \\ \psi_c - \psi_o & \text{if } \psi_i > \psi_o \end{cases} \end{aligned} \quad (15)$$

320 We use this formulation to discuss some of the unphysical implications for root water
 321 uptake from the former SMS parameterization of water stress (Equation 15).

322 3.1 Constant pulling potential

323 With SMS, that gradient is defined for each soil layer as the difference between the
 324 soil water potential in that layer (ψ_i) and a constant parameter, the soil water potential when
 325 stomata are fully closed (ψ_c). This parameter serves as the vegetation "pulling" potential for
 326 calculating the soil transpiration sink. Using a constant wilting point is inconsistent with ex-
 327 tensive evidence from the field of dynamic vegetation water potential, and cohesion tension
 328 theory (CITATIONS NEEDED) driving the transpiration flow. Likewise the values for ψ_c
 329 are quite negative, (-2.5 MPa for broadleaf evergreen tropical, BET, forests). Fisher *et al.*
 330 [2006] measured midday stem potential consistently higher than -0.5 MPa during the wet
 331 season, and on average -1.69 and -1.53 MPa during the dry season in the control and exclu-
 332 sion plots, respectively.

333 3.2 Conductance dynamics

334 In SMS, in lieu of dynamic vegetation water potential, intra-day SMS soil sink dynam-
 335 ics derive from a highly variable conductance (CLARIFY). As inferred in Equation 15, SMS
 336 conductance is modeled as a function of T_{\max} , and three constant parameters. T_{\max} is highly
 337 dynamic, responding to the diurnal course in transpiration demand. This is inconsistent with
 338 general principles of porous media flow, where conductivity is a function of the hydraulic
 339 architecture and its wetted status. Likewise, this representation of conductance does not rep-
 340 resent the characteristic phenomenon where vessels lose conductance with drying.

341 3.3 No dependence on belowground carbon allocation

342 As is typical in water stress parameterizations, the SMS conductance is scaled by layer
 343 using an area basis, here using the relative vertical root fraction is used. With PHS, an abso-
 344 lute measure of root biomass is used (see Appendix Equation B.7), so that the belowground
 345 water cycle interacts with carbon allocation to the roots. An absolute measure better con-
 346 forms with the physics of porous media flow and better responds to varying carbon allocation
 347 strategies. For example, with SMS, if root mass doubles in every soil layer, the root access to
 348 water remains unchanged.

349 3.4 Lacks penalties for extraction from depth

350 Both PHS and SMS account for the effect of decreasing root area with depth (PHS,
 351 root area; SMS, root fraction), but PHS implements two other penalties for extracting water
 352 from deep in the soil column that are missing from SMS. The first is minor, but water ex-
 353 tracted from depth must overcome gravity, amounting to about 0.01 MPa per meter in depth.
 354 This is missing from SMS and included with PHS. Likewise, SMS ignores the fact that hy-
 355 draulic conductance is generally taken to scale with the inverse of conducting length. Deeper
 356 roots feature longer root tissue conducting length, and root spacing within the soil is less
 357 dense, requiring longer conducting distances across the soil matrix. In PHS, both these pro-
 358 cesses result in diminished hydraulic conductance (UNCLEAR).

359 3.5 Constraints

360 With SMS, the gradient in water potential is constrained between 0 and the range of
 361 soil potential between parameters for stomata fully open and closed (Equation 15). The up-
 362 per constraint caps the gradient in water potential when soil potential reaches the value for
 363 stomata fully open ($\psi_o = -0.65$ MPa for BET). Darcy's Law predicts that the gradient in water
 364 potential would continue to increase until saturation matric potential. The lower constraint
 365 caps the gradient in water potential at zero, disallowing negative gradients. However, re-
 366 versed water fluxes, caused by positive gradients in water potential from root to soil, have
 367 been observed in the field [Burgess *et al.*, 1998]. Both constraints are eschewed with PHS.

368 4 Experiment Description

369 All four simulations in this paper use the same development version of CLM5 (devel-
 370 opment version r270, https://github.com/ESCOMP/ctsm/releases/tag/clm4_5_18_r270). The
 371 four simulations are used to assess the impact of the plant hydrodynamics model (PHS vs.
 372 SMS) on a through-fall experiment (i.e., with either ambient or 60% through-fall excluded),
 373 with all other model components and forcing shared. Simulations are run offline, spanning
 374 from 2001 through 2003, utilizing the satellite phenology mode of CLM5. All simulations
 375 start from the same initial conditions, which are the results of a 9-year spin-up repeating the
 376 PHS/Ambient simulation three times. To avoid duplication, descriptions of site characteris-
 377 tics, forcing data, and observational sap flux, can be found in Fisher *et al.* [2007].

378 4.1 Parameter Values and through-fall Exclusion

380 Select parameter values concerning vegetation hydrodynamics are presented in Table
 381 1. All other parameters use the default values associated with the r270 version of CLM5.
 382 Informed by Fisher *et al.* [2008], we tuned soil hydraulic parameters and through-fall exclu-
 383 sion to better capture the observational soil water dynamics (Fisher *et al.* [2007] Figure 4),
 384 Supplementary Figure A.1. Likewise, we tuned k_{max} and g_1 parameters to improve the fit
 385 to sap flux observations in the ambient simulation. The object of this paper is to present the
 386 dynamical impact of PHS to clearly describe model functionality. Model skill and parameter
 387 sensitivity will be assessed in follow-up studies.

388 5 Analysis Details

389 5.1 Water potential

390 Annual and diurnal cycles of vegetation water potential are presented. For the diurnal
 391 cycle, we average by timestep over the 91 days of SON, 2003, reporting curves for root, stem,
 392 shade-leaf, and sun-leaf water potential. For the annual cycle, we plot monthly mean midday
 393 (local time 12:00 to 14:00) sun-leaf water potential.

379

Table 1. Select parameter values

CLM name	Full Name	Symbol	Value
kmax(1)	Maximum Sun Branch Conductance	$k_{1a,\text{max}}$	4e-7 s ⁻¹
kmax(2)	Maximum Shade Branch Conductance	$k_{1b,\text{max}}$	4e-7 s ⁻¹
kmax(3)	Maximum Stem Conductivity	$k_{2,\text{max}}$	4e-7 m/s
krmax	Maximum Root Conductivity	$k_{r,\text{max}}$	6.3e-9 m/s
psi50	Water potential at 50% loss of conductivity	ψ_{50}	-2.45 MPa
ck	Vulnerability shape parameter	c_k	3.95
smpso	Soil potential with stomata fully open	ψ_o	-0.647 MPa
smpsc	Soil potential with stomata fully closed	ψ_c	-2.5 MPa
medlyn_intercept	Medlyn intercept	g_0	100 $\mu\text{mol} / \text{m}^2 / \text{s}$
medlyn_slope	Medlyn slope	g_1	7 kPa ^{0.5}
n	Soil porosity	n	0.42
hksat	Saturated soil hydraulic conductivity	$k_{s,\text{max}}$	1.5e-5 m/s
sucsat	Saturated soil matric potential	ψ_{sat}	461 Pa
bsw	Brooks-Corey parameter	b	6

^aTable note text here.

401

Table 2. Root-zone soil potential terciles for Figure 5

Simulation	T1	T2
PHS, Ambient	-0.0136 MPa	-0.0476 MPa
PHS, TFE	-0.0788 MPa	-0.2454 MPa
SMS, Ambient	-0.0056 MPa	-0.2296 MPa
SMS, TFE	-0.6474 MPa	-1.8467 MPa

394

5.2 Stress factor, annual cycle

395
396
397
398
399

Monthly means are reported for transpiration, gross photosynthesis, and f_w , the water stress factor (Fig 3). For the water stress factor, we opt to report the midday water stress averaging over local time 12:00 to 14:00. Monthly mean observational sap flow is also shown, courtesy of *Fisher et al. [2007]*, which reports details on scaling observations to stand level. Months were dropped that featured fewer than 5 days of data.

400

5.3 Stress factor, diurnal cycle

402
403
404
405
406
407
408
409
410
411

In Figure 4, we plot the diurnal cycle of the stress factor averaged over the 2003 dry season (SON) (I am not a big fan of sentences in Figure we show, better to say what ahppens and then refer to figure). Drivers of the stress function are examined in Figure 5. To highlight the response of stress to VPD, we subsetted data according to downwelling solar radiation, which also influences stress. Data are selected with downwelling solar radiation between 400 and 425 W/m², which corresponds to 775 half-hour timesteps. For the TFE simulations, (Figure 5c,d), we additionally exclude data from 2001, because TFE was not initiated until November 2001, leaving 515 timesteps. Data are subdivided into terciles based on soil water (within each plot), and colored accordingly. The terciles are defined for each simulation in Table 2.

412 5.4 Hydraulic conductance

413 In Figures 6 and 7, we compare conductance values derived from the PHS and SMS
 414 implementations. With SMS, k is not explicitly modeled, so instead we infer k , by dividing
 415 root water uptake q_i , by $\Delta\psi$ as defined in Equation 15. We interpret the constraint that $\Delta\psi$
 416 be greater than or equal to zero to mean that conductance is zero in non-conforming cases,
 417 which we extend to $k = 0$ when $\Delta\psi < 1$ kPa. For our analyses, we consider only points
 418 when transpiration is greater than 4 W/m², which improves the tractability of inferring con-
 419 ductance, given that SMS root water uptake is precluded absent transpiration (REPHRASE).

420 For Figure 6a,b, conductance is plotted from Soil Layer 3 (spans from 6 to 12 cm be-
 421 low ground), for all points during 2003 when transpiration is greater than 4 W/m² (n=7752).
 422 For Figure 7a,b, conductance is averaged daily, subject to the same restrictions. Average
 423 intra-day standard deviation is reported for FMA, by which we calculate a daily standard de-
 424 viation of complying points, and report the average over the 89 days.

425 5.5 Root water uptake

426 Vertical profiles of the rate of root water uptake are presented in Figures 8a and 9a, av-
 427 eraged over SON and FMA, respectively. This is plotted as average cumulative rate of root
 428 water uptake, starting at depth (8.6 meters). Time series of total root water uptake are also
 429 provided (Figs 8b,c, 9b,c). We plot total cumulative water extracted from near the surface
 430 over time in Figures 8b and 9b, accompanied by that extracted from depths beyond 20 cen-
 431 timeters in Figures 8c and 9d. We chose 20 centimeters as the break point based on the ver-
 432 tical profiles of root water uptake, and with a preference for not splitting any of the discrete
 433 soil layers. Soil Layers 1-4 span 0 to 0.2 meters, and Soil Layers 5-20 span 0.2 to 8.6 meters.
 434 Time series of total cumulative ambient precipitation are shown for comparison (Figs 8b and
 435 9b).

436 5.6 Hydraulic redistribution

437 Hydraulic redistribution refers to flows of water between soil layers through vegetation
 438 substrate, resulting in water deposition in lieu of water uptake. To calculate total HR, we
 439 take the sum across all soil layers of only negative root water uptake fluxes (multiplied by the
 440 model timestep duration, 1800 seconds). For Figure 10 we partition by month and by local
 441 time: at night (summing from 6p.m. to 6a.m.), and during the day (6a.m. to 6p.m.). Note
 442 that, over the course of a day or season, HR can occur without net negative root water uptake.
 443 For example, hydraulic lift may occur at night, depositing deep water near the surface, which
 444 is then transpired during the day, resulting in HR alongside net positive root water uptake.
 445 This is evident in Figure 8, where there is net positive root water uptake throughout the soil
 446 column over the 2003 dry season, alongside significant HR (Fig 10).

447 5.7 Soil moisture

448 The vertical profile soil water potential under 60% TFE is plotted in Figure 11 (SMA,
 449 DO NOT SAY THIS IS PLOTTED BUT DESCIRBE RESULTS AND MENTION FIG-
 450 URE). The range in soil potential is much larger within the SMS paradigm, which made it
 451 difficult to plot both panels with the same color scale. In order to preserve information in
 452 the PHS plot, we opt for a scale of 0 to -1 MPa, as compared to 0 to -3 MPa for SMS. When
 453 comparing column average soil potential, we use separate definitions, which reflect each
 454 paradigm's representation of soil water availability. With SMS, we opt for a root-fraction
 455 weighted average, following from Equation 14. This is a poor measure for PHS, because it
 456 neglects gravitational contributions and the appropriate root area basis. Instead we opt for
 457 predawn (defeined at 5AM) root water potential, which, given minimal transpiration, is in
 458 equilibrium with the soil column.

459 **6 Results and Discussion**

460 **6.1 Modeling vegetation water potential**

461 The models are compared during for the 2003 dry season (SON) at Caxiuana for two
 462 experiments: the first with ambient rainfall, and the second with 60% of rainfall excluded,
 463 Figure 2. In the ambient simulation (Fig 2a), average midday water potentials are -1.96, -
 464 1.95, -1.94 MPa for sunlit leaf, shaded leaf, and stem, respectively. With through-fall exclu-
 465 sion (TFE), midday water potentials decrease to -2.77, -2.76, -2.75 MPa, respectively (Fig
 466 2b).

467 Both panels show the characteristic drop in water potential around midday and the ex-
 468 pected sequencing with the leaf water potentials more negative than the stem potential, which
 469 is more negative than the root potential. The sequencing is difficult to distinguish from the
 470 plot, where the stem, sunlit, and shaded leaf water potential curves nearly overlap for both
 471 experiments because there is only very small drop between the stem and leaves. The small
 472 difference between leaf and stem water potentials results from minimal resistance to water
 473 flow across these segments. (LINK THIS TO THE PREVIOUS STATEMENT) The current
 474 PHS parameterization of stem-to-leaf resistance is relatively simple compared to the litera-
 475 ture [Franks *et al.*, 2007] and could be advanced in future versions.

476 TFE lowers average midday sunlit leaf water potential by 0.81 MPa compared to the
 477 ambient simulation, during SON-2003 (dry season). This change in water potential can
 478 be partitioned among: change in soil potential, change in potential drop from soil-to-root,
 479 and change in potential drop from root-to-leaf. In the ambient simulation, average predawn
 480 (5AM) root water potential (an integrated measure of soil water potential) is -0.075 MPa.
 481 With TFE, it falls to -0.36 MPa, resulting in a decrease in predawn root water potential of
 482 0.28 MPa relative to the ambient simulation. The difference between midday and predawn
 483 root water potential (which stands in for potential drop from soil-to-root) lowers by 1.06 MPa
 484 with TFE (from -0.06 MPa, ambient, to -1.12 MPa, TFE). The difference between sunlit leaf
 485 and stem water potential at midday acts in the opposite direction, changing from -1.83 MPa
 486 in the ambient simulation to -1.29 MPa with TFE, attenuating the drop in leaf water potential
 487 by 0.54 MPa.

488 Predicted water potential values are comparable with field observations, where average
 489 dry season leaf water potential was measured as -2.47 MPa [Fisher *et al.*, 2006]. With PHS,
 490 modeled change in leaf water potential due to TFE is -0.81MPa, which can be partitioned
 491 into -0.28 MPa predawn root water potential, -1.06 soil-to-root drop, +0.53 root-to-leaf drop.
 492 The drop in water potential across the stem partially abates the change in the soil and roots
 493 due to TFE. Though stem conductance decreases with drying, transpiration also decreases,
 494 yielding a net effect of a smaller drop in water potential across the stem. This is consistent
 495 with findings in Fisher *et al.* [2006] that most of the whole-plant resistance is above ground,
 496 but that added resistance from drying is predominately below ground. Likewise Fisher *et al.*
 497 [2006] found evidence of isohydric behavior, where plants manage water loss through stom-
 498 ata to regulate leaf water potential, which is consistent with results here of reduction in po-
 499 tential drop across the stem. However, where our experiment features declines in leaf water
 500 potential due to TFE, Fisher *et al.* [2006] found no significant difference between ambient
 501 and TFE dry season. This could indicate that our parameters do not result in sufficiently iso-
 502 hydric behavior.

503 Many facets of our hydraulic representation are simplified relative to the literature,
 504 reflecting that, in a model set to run at the global scale, there is a tradeoff between added
 505 complexity and parameter reduction. The current PHS parameterization omits vegetation
 506 capacitance, which may be important for accurately modeling the diurnal cycle of water
 507 stress especially in tropical rainforests [Meinzer *et al.*, 2009]. Hydraulic conductance hys-
 508 teresis and permanent cavitation are absent from the PHS vulnerability parameterization,
 509 whereby xylem segments fully regain conducting capacity upon re-wetting. This limits the

510 influence of drought legacy, which has been shown to be significant for forest mortality [An-
 511 dregg *et al.*, 2013b]. Similar to other simplified models [Xu *et al.*, 2016], loss of conduc-
 512 tance is based on lower terminus water potential, which may underestimate integrated loss of
 513 conductivity [Sperry and Love, 2015]. These simplifications each serve to lessen the param-
 514 eter and/or computational burden of PHS. Our objective was to simplify the plant hydraulic
 515 representation for this first implementation, allowing that it will be of interest to investigate
 516 more extended process representation in future versions.

517 6.2 Stress factor, annual cycle

518 Figure 3 shows monthly mean values of the water stress factor, gross primary produc-
 519 tivity, and transpiration over the three-year simulations for PHS versus SMS under ambient
 520 and 60% through-fall exclusion conditions. Under ambient through-fall conditions, the SMS
 521 simulation features less stress (Fig 3b), with no stress ($f_w > 0.99$) in 24 out of 36 months.
 522 PHS predicts more stress (Fig 3a), with stress in sync with the evolution of midday leaf water
 523 potential (Figure 2). As a result, f_w is generally lowest in September (Fig 3e). ZQZ need to
 524 go back and output btran proper. Alternatively, SMS predicts no stress ($f_w > 0.99$) during any
 525 of the three Septembers of the ambient simulation. Instead f_w is generally lowest in Decem-
 526 ber.

527 Both stress parameterizations attenuate V_{cmax} based on vegetation water status, regu-
 528 lating photosynthesis and transpiration (WASN'T THERE SOMETHING INCONSISTENT
 529 BEFORE). The difference is in how they diagnose water status: SMS uses a function of soil
 530 potential, and PHS uses a function of leaf water potential. SMS has the most stress in De-
 531 cember, which is associated with lower soil moisture (Supp Fig ??). While soil moisture is
 532 lowest in December, transpiration demand is higher in September, which is the month with
 533 the most stress in the PHS simulations (Fig3a). To achieve high transpiration rates, vegeta-
 534 tion must operate with a large gradient in water potential from soil-to-leaf, associated with
 535 increased xylem tension and risk of cavitation. As such, leaf water potential declines with
 536 soil moisture drying, but also with increasing transpiration demand (Fig 2). PHS is designed
 537 to represent hydraulic limitation to transpiration associated with xylem tension, which re-
 538 sponds to both soil drying and increased transpiration demand (i.e. higher VPD) [Sperry and
 539 Love, 2015]. The latter was absent from the SMS formulation.

540 Hydraulic limitation establishes a negative feedback loop between photosynthesis/transpiration
 541 and water stress. As an example of the negative feedback, if photosynthesis increases, gener-
 542 ally stomatal conductance and transpiration increase. This causes more negative leaf water
 543 potential and an associated increase in water stress, which attenuates photosynthesis. This
 544 diminishes variability in transpiration and photosynthesis, relative to SMS (Fig 3c-f). The
 545 strength of this feedback is subject to parameters controlling maximum conductance and
 546 the stomatal response to leaf water potential. Quantifying variability in diffusive fluxes with
 547 PHS as compared to SMS and observations is an important topic for future studies.

548 through-fall exclusion (which initiates on November 1, 2001) adds stress in both the
 549 SMS and PHS simulations (Fig3c,d) . The added stress is greater and onset faster with SMS.
 550 In both cases, the effect of TFE accumulates in time, with less photosynthesis and transpi-
 551 ration in 2003 compared to 2002. This is not reflected in the sap flux observations, which
 552 feature a more rapid onset of reduced transpiration, and similar transpiration between 2002
 553 and 2003.

554 In both SMS and PHS, soil water is used to buffer shortfalls in precipitation versus
 555 transpiration (Supp Fig A.9). (UNLCEAR) This effect may be overestimated in the model,
 556 contributing to delayed stress onset relative to observations. PHS is less sensitive to TFE,
 557 which can be partly attributable to differences in root water uptake (see Section 6.5). Indeed,
 558 PHS utilizes more deep soil water to mitigate declines in root-zone soil moisture as water
 559 flow is imposed to go down water potential gradients. In the dry season surface drying also
 560 decreases soil-root conductance so that it is easier to extract moisture from deeper layers,

consistent with observations based on isopotes (CITATION). Significant uncertainty exists in soil and root hydraulic parameters as well as the root distribution, whereby better behavior may exist within the plausible parameter space. Likewise, the parameter values for both stress implementations could be tuned further. Observations indicate the trees here adopt an isohydric behavior, where declines in soil moisture are tightly coupled with reduced transpiration, which mitigates decreases in leaf water potential [Fisher *et al.*, 2006]. The parameter values employed for these simulations may be insufficiently isohydric (GIVE REFERENCE AND DEFINE ISOHYDRICITY), which could explain limited sensitivity to TFE relative to observations.

6.3 Stress factor, diurnal cycle

In addition to changes in the annual cycle, PHS introduces a diurnal cycle to f_w (Fig 4a). The SMS version of f_w exhibits little diurnal variability (Fig 4b). The difference between paradigms follows from the functional inputs. SMS models water stress a function of soil water potential, which lacks a diurnal cycle. Instead, PHS uses a function of leaf water potential (e.g. Fig 2a,b) to model water stress. Leaf water potential declines with decreasing soil potential, but also with increasing transpiration demand. Transpiration demand is a function of VPD, solar radiation (via photosynthesis), and other variables, which impart a diurnal cycle.

The relationship of water stress with VPD and soil potential is shown in Figure 5. To emphasize the relationship with VPD, data are subsetted for a small window in downwelling solar radiation (between 400 and 425 W/m²). For the TFE simulations (panels *c* and *d*), we also subset for years 2002 and 2003, because TFE was not active during most of 2001. Points are colored based on soil potential, partitioning the data from each plot into terciles, blue points are wettest, red points driest, and yellow points intermediate. For details on the soil water classification and radiation subsetting see Section zqz (THIS SHOULD BE IN CAPTION NOT MAIN TEXT).

The SMS version of f_w has a clear dependence on soil potential, but no relationship with VPD (Fig 5b,d), as expected. Drier soil potentials are associated with lower values of f_w (which corresponds to more stress). With PHS, higher VPD results in more stress (Fig5a,c). Under ambient through-fall conditions (Fig5a), soil water potential has minimal influence. With TFE, stress responds to both VPD and soil water (Figure 5c). Similar effects are shown in response to downwelling solar radiation (Supp Fig A.2).

Water stress is applied to capture limitations with declining water status that are not reflected within stomatal optimization theory. CLM implements non-stomatal limitation by multiplying V_{cmax} by f_w . Though there is limited evidence of down-regulation of V_{cmax} [Flexas *et al.*, 2006], this was the best option within CLM for applying stress through the GPP term of the stomatal conductance model, in accordance with field observations [Lin *et al.*, 2018; Zhou *et al.*, 2013]. If in future versions of CLM, mesophyll conductance is represented, it may be a more appropriate avenue for achieving the same effect. (MERGE WITH PREVIOUS DISCUSSION, TRY AVOIDING REPETITIONS A MUCH AS POSSIBLE)

Total soil water content (or departure from saturaiotn) is a typical basis for diagnosing water status and sterss [Drake *et al.*, 2017], which is in line with an SMS-type approach. While capturing supply limitations, this framework neglects effects of transpiration demand on xylem tension. Given constant stomatal conductance, xylem tension increases with declining soil water, but also with increasing vapor pressure deficit. While VPD sensitivity is included in the Medlyn model, it serves to mitigate increasing water costs, without consideration of cavitation. Evidence suggests that vegetation employ water use strategies to mitigate the risk of cavitation associated with increasing xylem tension [Sperry *et al.*, 1998; Fisher *et al.*, 2006; Choat *et al.*, 2012]. Utilizing leaf water potential as the basis for water status reflects this constraint. This may be especially important given projected increases in VPD associated with warming.

612 6.4 Hydraulic conductance

613 Soil-to-root conductance (k_{sr}) is explicitly represented in PHS, modeled as a function
 614 of soil potential (ψ). With SMS, k_{sr} is not explicitly modeled, but it can be inferred, by
 615 dividing root water uptake by the gradient in water potential (see Section zqz). Comparing
 616 conductance under these two paradigms serves to highlight differences in how water supply
 617 is modeled. In , we plot the time-series of conductance values from Soil Layer 3 (spanning
 618 from 6 to 12 centimeters below the surface) under ambient through-fall conditions during
 619 2003, along with precipitation over the same period (PLUG IN CAPTION).

620 During the wet season, PHS conductance is greater than SMS by more than two orders
 621 of magnitude (Fig 6a,b). PHS conductance is generally steady through the wet season (Fig
 622 6a), followed by a steady decline over the dry season with short resurgence episodes associ-
 623 ated with rain events. SMS conductance features more variability relative to the mean (Fig
 624 6b). During FMA-2003, average intra-day standard deviation of Layer 3 conductance is $4.6 \cdot 10^{-12} \text{ s}^{-1}$ with PHS and $9.9 \cdot 10^{-12} \text{ s}^{-1}$ with SMS. In an absolute sense the SMS standard deviation
 625 is about twice as large as PHS. The difference is larger in a relative sense, as this corresponds
 626 to 0.08% of the mean FMA conductance with PHS and 62.9% of the mean FMA conduc-
 627 tance with SMS.

629 The SMS inferred conductance is tethered to transpiration (see Section 3), which leads
 630 to the high variance and a clear diurnal cycle (Supp Fig A.3). Instead PHS calculates k_{sr}
 631 based on soil hydraulic properties and root xylem vulnerability, which better reflects the
 632 physics (flow has to be down water potential gradients) and the temporal dynamics of tran-
 633 spiration demand. As a result conductance is less variable, with the expected responses
 634 to drydown (loss of conductance) and re-wetting (increased conductance). This is further
 635 demonstrated in Figure 7, where we plot the daily mean conductance from Soil Layer 3.
 636 With 60% through-fall exclusion (Fig7a, dotted line), PHS conductance decreases, whereas
 637 with SMS, the daily mean conductance increases (Fig7b). The latter SMS increase is un-
 638 realistic and conflicts with extensive literature demonstrating loss of conductivity with drying
 639 (CITATIONS).

640 Despite two orders of magnitude difference in conductances, total root water uptake
 641 during FMA2003 is not very different (23.4 cm PHS vs. 24.9 cm SMS). The reason in these
 642 smaller differences, is that extraction gradient compensate for the differences in conductance.
 643 The SMS extraction gradient is measured relative to ψ_c (a parameter defining soil potential
 644 with stomates fully closed), which equals -2.5MPa for BET. The PHS extraction gradient is
 645 relative to root water potential which during 2003 (ambient through-fall) varies between -
 646 0.02 and -0.23 MPa. Fisher *et al.* [2006] measured stem water potential consistently higher
 647 (less negative) than -0.5MPa.

648 With TFE, PHS Layer 3 conductance can approach the values seen in SMS. The aver-
 649 age Layer 3 conductance with PHS for August 2003 (60%TFE) is $4.75 \cdot 10^{-11} \text{ s}^{-1}$ as compared
 650 to $3.89 \cdot 10^{-11} \text{ s}^{-1}$ for SMS. This is a result of the orders of magnitude response of PHS soil-to-
 651 root conductance to changes in soil potential (Supp Fig A.4) (UNCLEAR MODIFY SEN-
 652 TENCE). This conforms with typical soil hydraulics, where large changes in conductance
 653 occur with drying. On the other hand, SMS conductance has no clear relationship with soil
 654 potential (Supp Fig A.4).

655 6.5 Root Water Uptake

656 Hydraulic conductance is used to model root water uptake, the flux of water (q_i , mm/s)
 657 extracted from each of the vertically discretized soil layers ($i = [1, 2, \dots, n]$). These fluxes are
 658 used as the soil transpiration sink terms within the Richards' equation [Oleson *et al.*, 2013]
 659 and, summed over the soil column, are equivalent to the transpiration flux. As described
 660 above (and in Section 3), PHS adopts a hydraulic framework for root water uptake.

661 PHS simulations (black color), feature more surface extraction than with SMS, espe-
 662 cially under ambient through-fall conditions (Fig8a), during the 2003 dry season. The time-
 663 series of PHS total cumulative extraction (cm) from near-surface soil (Fig8b) responds to
 664 precipitation (Fig8d), with increased surface extraction after rain events. Under ambient con-
 665 ditions the SMS partitioning of extraction between near-surface and depth is not sensitive to
 666 precipitation. PHS near-surface extraction decreases by 40% with TFE (8.12 vs 13.51 cm),
 667 while, SMS features a 24% increase (5.28 vs 6.55 cm, Fig 8b). Under TFE, both PHS and
 668 SMS extract minimal water from between 0.5 and 4m, (3.18 cm and 0.56 cm, respectively,
 669 over the three months). Both compensate by increasing extraction from below 4m, but PHS
 670 to a much larger extent, which corresponds to overall significantly more root water uptake
 671 during TFE.

672 Root water uptake dynamics respond to changes in hydraulic conductance and/or changes
 673 in the gradient in water potential. With decreasing soil potential, hydraulic conductance de-
 674 creases with PHS, but can increase with SMS (6.4). SMS is limited by the extraction gra-
 675 dient, with root water uptake declining to zero as soil potential approaches -2.5 MPa (Supp
 676 Fig A.5). PHS is more sensitive to changes in soil water potential, with stronger decreases
 677 in root water uptake in response to drying within a soil layer (Supp Fig A.5). PHS features
 678 increases in near-surface water uptake after rain and decreases with TFE. SMS near-surface
 679 water uptake is less sensitive to rain events and increases with TFE.

680 PHS has more access to water at depth under TFE, associate with higher conductance
 681 values.

682 The wet season (FMA-2003), features more and steadier rain (Fig 9d). PHS responds
 683 with an increase in the proportion of water extraction from near the surface relative to SON.
 684 Under ambient conditions net extraction is zero beyond about 38 centimeters (Fig 9a, solid
 685 black line). In comparison, SMS extracts more than half its water from beyond 1 meter in
 686 depth (Fig 9a, solid gray line). With TFE, PHS extraction is negative beyond 20 centimeters
 687 (Fig 9c), whereby over FMA-2003, there is no net root water uptake beyond 20 centimeters,
 688 but rather deposition of about 10 cm of water.

689 In both the wet and dry season, PHS features significantly more root water uptake from
 690 the near-surface layers (0 to 20cm in depth). Modeled surface extraction is especially high
 691 over the wet season under through-fall exclusion conditions, summing to 32.7 cm over 89
 692 days. With a soil porosity of 0.42, the top 20 cm of soil hold only 8.2cm of water at satu-
 693 ration. By comparison SMS extracts 4.8 cm under the same conditions. Conductances are
 694 higher with PHS (see Section 6.4), which allows for higher rates of root water uptake, espe-
 695 cially from moist soil layers. Likewise PHS better reflects penalties for extraction from depth
 696 (Section 3, favoring near-surface water. The highest rates of root water uptake (relative to
 697 layer size) occur from Soil Layer 2, after rain events during the dry season (Supp Fig A.7).
 698 Lowering maximum conductance can attenuate high rates of extraction, if observations con-
 699 flict with model output.

700 During the wet season surface extraction supplies transpiration, but also is also re-
 701 distributed into lower soil layers. Hydraulic redistribution has been observed in the field
 702 [Oliveira *et al.*, 2005], and is an important missing feature from CLM [Lee *et al.*, 2005]. This
 703 functionality is precluded with SMS, which sets root water uptake to zero if the gradient in
 704 water potential is negative. Hydraulic redistribution with PHS is discussed further in the next
 705 section.

706 Finally, comment on SMS vs. PHS overall SMS has bad dynamics, but offers guardrails
 707 Modeling vwp allows for more realistic physics Both are difficult to parameterize and have
 708 many DOF. Observations of states and fluxes are sparse. PHS also offers a process connec-
 709 tion between soil potential and leaf water potential. Clear we need better ways to constrain
 710 root water uptake with observations. You can mention isotopes even if they are tricky. For
 711 instance cite recent work of INez Fung and Eel creek.

712 6.6 Hydraulic redistribution

713 Under ambient conditions HR totals to 41.3 cm (10.3 cm during the day, 31.0 cm at
 714 night), Figure 10. HR declines slightly to 37.0 cm (11.5 cm day and 25.5 cm night) with
 715 TFE. For reference, total transpiration over the same time period was 120 and 99 cm for am-
 716 bient and TFE conditions, respectively. The TFE simulation has less HR overall, but more
 717 HR during wet months, Feb-June.

718 More HR occurs at night, in accordance with observations and theory [Oliveira *et al.*,
 719 2005; Lee *et al.*, 2005]. For HR to occur into a soil layer, the soil potential must be more
 720 negative than the ψ_{root} (see Figure . During the day, transpiration requires a gradient in water
 721 potential from soil-to-root, which lowers ψ_{root} , decreasing the amount of HR. Increased HR
 722 with TFE occurs in Feb-June, associated with the drier TFE soils and larger gradients in soil
 723 potential from surface to depth. HR is lower in January, and July-December with TFE. Simi-
 724 lar to during the wet months the gradient in soil potential (in this case from depth to surface)
 725 is larger with TFE. However, the soils overall are so dry with TFE during the dry months,
 726 that loss of conductance from soil-to-root counteracts the large gradient, resulting in lower
 727 HR.

728 HR is predominately downwards during the wet season (FMA), serving to diminish the
 729 gradient between the newly-wetted surface and still-dry depths (Supp Figs A.6,A.7). Redis-
 730 tribution occurs in both directions during the dry season (SON), downwards after rain events,
 731 and upwards with drying. Only with TFE, and only during the dry season, is there significant
 732 extraction beyond 6 meters (Figs 8, 9). There is very little water deposited at depths beyond 6
 733 meters at any point in either simulation.

734 HR has been observed in the field [Oliveira *et al.*, 2005] and has been shown to mod-
 735 ify seasonal climate [Lee *et al.*, 2005]. The SMS paradigm, precludes the occurrence of HR
 736 [Oleson *et al.*, 2013]. The dynamics of HR with PHS align with observations, with more HR
 737 at night, and HR occurring in both directions vertically [Burgess *et al.*, 1998]. The absolute
 738 values of HR are difficult to assess, given limited observations. Allowing HR to occur into
 739 the top layer of the soil column significantly degraded modeled soil evaporation (not shown).
 740 We opted to omit the first top Layer (spanning 0 to 2 cm below ground) soil-to-root hydraulic
 741 conductance, to prevent HR from over-supplying water for soil evaporation.

742 Is hydraulic redistribution a feature or a liability? HR is a natural consequence of using
 743 Darcy's Law to model root water uptake - when gradients are reversed, HR should occur. as
 744 such it is naturally included within a plant hydraulics model with multiple soil layers and is
 745 an emergent behavior of respecting hydraulic flow down gradient of potentials. Still, HR is not
 746 represented in many models, even when based in hydraulic theory [Xu *et al.*, 2016; Christof-
 747 fersen *et al.*, 2016]. Most literature models force the model with a single soil water potential
 748 ψ_s , which precludes HR [Fisher *et al.*, 2007; Bonan *et al.*, 2014; Sperry *et al.*, 2017], which
 749 we have shown can substantially affect the seasonal cycle of water fluxes. Christoffersen *et al.*
 750 [2016] expand beyond a single ψ_s horizontally, but still feature a single soil layer in the ver-
 751 tical. However, in ESMs, soil moisture is typically resolved vertically and thus interfacing
 752 the plant hydraulics with a multi-layer soil naturally account for HR. Other models, similar to
 753 the SMS paradigm, disallow HR by constraining root water uptake to be positive [Xu *et al.*,
 754 2016]. Likewise HR is likely sensitive to the representation of vegetation tissue capacitance
 755 and below-ground hydraulic segmentation (CITATIONS NEEDED).

756 6.7 Soil profile

757 The column total soil water in all four simulations is initialized at 2.66 meters (over an
 758 8.6-meter soil column) (SAY WHY). The change in total soil water is small under ambient
 759 conditions, decreasing by 0.3cm with PHS and 9.6cm with SMS over the three-year simula-
 760 tions. Root zone soil potential is lower with SMS, with a root-fraction-weighted average soil
 761 potential of -0.42 MPa during November 2003. The equivalent metric from PHS, average

762 predawn root water potential, is -0.08 MPa. Under 60% through-fall exclusion, the change
 763 in soil water is -1.12 meters with PHS and -0.94 meters with SMS, relative to the ambient
 764 simulations (Supp Fig A.9). With SMS, this corresponds to a root-fraction-weighted average
 765 soil potential of -2.18MPa during November 2003, whereas PHS average predawn root wa-
 766 ter potential is -0.37MPa (Figure 11). Observations of root-zone potential based on gravity-
 767 corrected predawn leaf water potential are -0.17 ± 0.10 MPa under ambient conditions, and
 768 -0.71 ± 0.31 MPa with through-fall exclusion [Fisher et al., 2007].

769 SMS simulations achieve more negative root-zone soil potential than with PHS. With
 770 60% TFE, the SMS root-zone is 1.81 MPa drier, despite having a slightly moister soil col-
 771 umn overall (1.61m total water vs. 1.54m for PHS). This is associated with differences in the
 772 parameterization of root water uptake. SMS operates with a larger gradient for water extrac-
 773 tion (see Section 6.4), which allows for more negative water potential in active soil layers.
 774 PHS has more access to deep soil water under dry conditions (Fig 8), which mitigates de-
 775 clines in soil potential near the surface. While PHS better matches observations of root-zone
 776 soil potential, we hesitate to make conclusions about model skill. This is due to parameter
 777 uncertainty and tuning (see Section 4.1), as well as the fact that both models feature high bi-
 778 ases in transpiration relative to observations.

779 Darcy's Law establishes that water flow is proportional to the gradient in total water
 780 potential. With PHS, this gradient is measured relative to dynamic ψ_{root} . With SMS, this
 781 gradient is measure relative to a constant parameter, ψ_c , the soil potential with stomates fully
 782 closed. This approach is required without prognostic vegetation water potential, but yields
 783 unsatisfactory dynamics that do not comply with the physics of porous media flow (see Sec-
 784 tion 6.4). Furthermore, it seems that ψ_c has historically been tuned for its effects on diffusive
 785 fluxes, without specific attention to the effect on soil moisture dynamics (Can someone else
 786 back me up on this? Is there a way to cite this?).

787 This is problematic, because soil moisture dynamics are very sensitive to ψ_c . Root wa-
 788 ter uptake halts when soil potential reaches ψ_c (Section 3), setting an effective minimum soil
 789 potential. This is visible in Figure 11, where, much of the plot features soil potential at -2.5
 790 MPa, the value of ψ_c . This is clearer in Figure A.11, where soil layers can be seen to dry out
 791 quickly, but not beyond -2.5 MPa (with the exception of Soil Layers 1 and 2, which are influ-
 792 enced by bare soil evaporation). The effect of ψ_c extends to ambient through-fall conditions
 793 (Fig A.10), but over a smaller spatial and temporal domain. PHS has more flexibility, due to
 794 dynamic root water potential, so there is not the same tendency to dry out to a certain level.
 795 Instead minimum soil potential for PHS gets lower each dry season throughout the TFE sim-
 796 ulation (Fig 11a).

797 Soil water dynamics in CLM are very sensitive to the representation of root water up-
 798 take. With PHS, because we're modeling vegetation water potential, we can utilize a hy-
 799 draulic framework, which offers a well-established physical basis and a clear improvement
 800 in model structure. SMS root water uptake has problematic model structure, seemingly no
 801 empirical basis, and intuitively does not look good on soil water dynamics. PHS improves
 802 model structure, but it also adds parameters that are difficult to constrain. Due to the scarcity
 803 of observational constraints, vertically-resolved soil moisture predictions are challenging to
 804 evaluate. PHS offers leaf and stem water potential observations, which are downstream of
 805 soil potential, and could be an exciting opportunity to interface with observations. While
 806 PHS seems a clear improvement over SMS, which does not comport well with fundamental
 807 aspects of hydraulic theory, further work on the representation of root water uptake in models
 808 is needed to validate both soil water states and fluxes.

809 **7 Conclusion**810 **7.1 Caveats**

811 Modeling stomatal conductance and photosynthesis, especially subject to water stress,
 812 is an area of ongoing research. We use the Medlyn model coupled to a hydraulic stress func-
 813 tion that attenuates V_{cmax} . This complies with observations [Lin *et al.*, 2018; Zhou *et al.*,
 814 2013] that stress applied through g_1 underestimates attenuation of photosynthesis. However,
 815 there is no direct evidence of declines in V_{cmax} with drought [Flexas *et al.*, 2006], whereby
 816 future work may seek to represent mesophyll conductance in CLM.

817 The model hydraulic supply representation is simplified, to reduce the model parameter
 818 and computational burdens. No capacitance. No integration of xylem or soil conductances
 819 vulnerability, instead based on lower node. No hysteresis in loss of conductance, xylem in-
 820 stantly regain conductance upon re-wetting. Leaf conductance simplified. Soil layers fully
 821 parallel, soil potential constant each time step.

822 Parameter uncertainty is significant. Notions of hydraulic architecture will never per-
 823 fectly fit on this modeling scale, especially in a PFT paradigm. Field measurements of hy-
 824 draulic traits will help constrain parameter ranges, but mostly only aboveground. Flux ob-
 825 servations can help to tune stress parameters. Parameter estimation for root functioning is
 826 significantly more challenging, given the difficulty in underground trait observations. Like-
 827 wise observational constraints of vertically-resolved states and fluxes underground are scarce.
 828 Follow-up work will be geared towards parameter estimation and assessing model skill.

829 **7.2 Utility of modeling vegetation water potential**

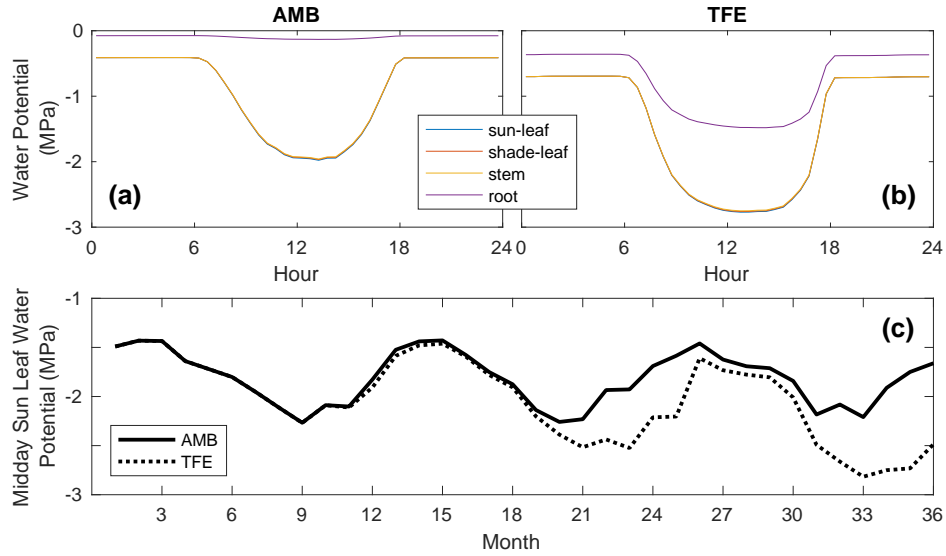
830 This will be the final conclusions. Any comments on overall takeaways?

831 PHS models vegetation water potential. This offers structural improvements for stress
 832 and for root water uptake. Stress now functions with hydraulic limitation. RWU now follows
 833 Darcy theory, incorporates HR, and responds appropriately to vegetation allometry.

834 **8 Acknowledgments**

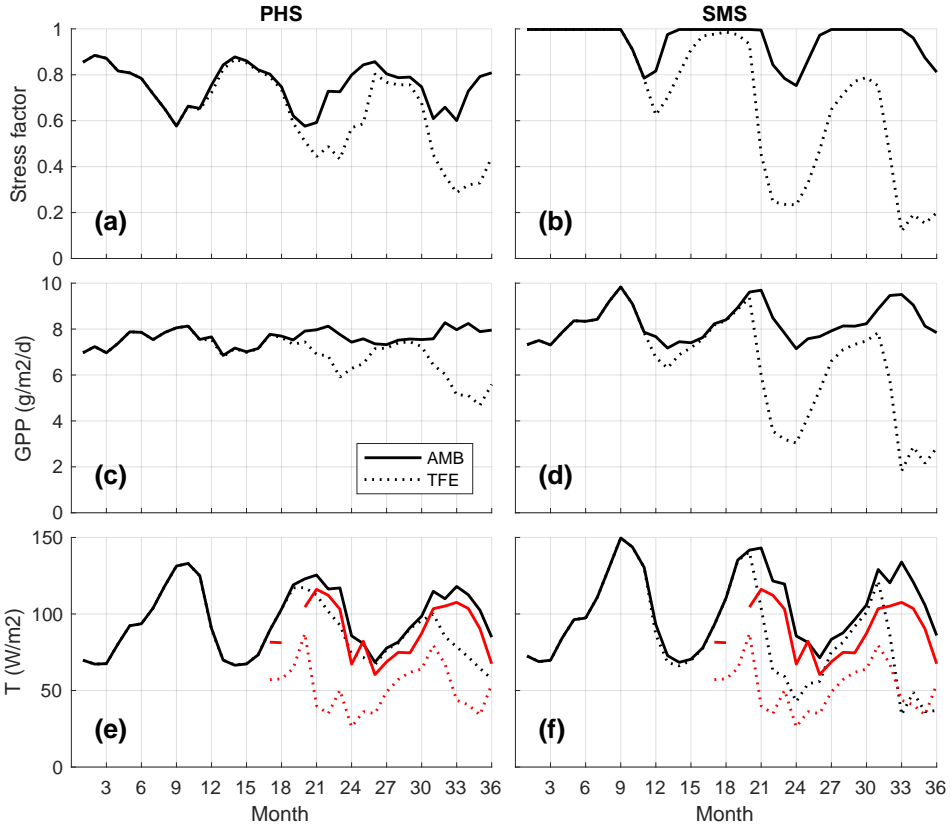
835

9 Figures

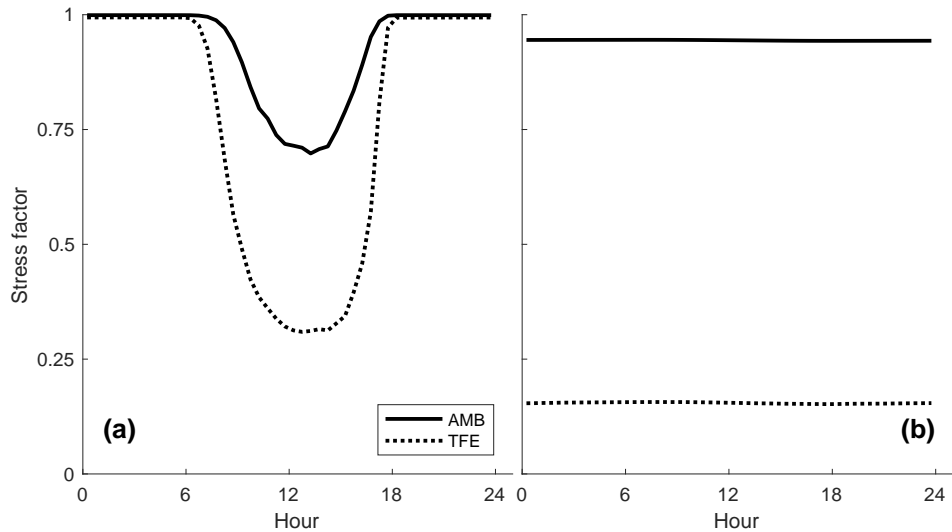


836
837
838
839
840
841

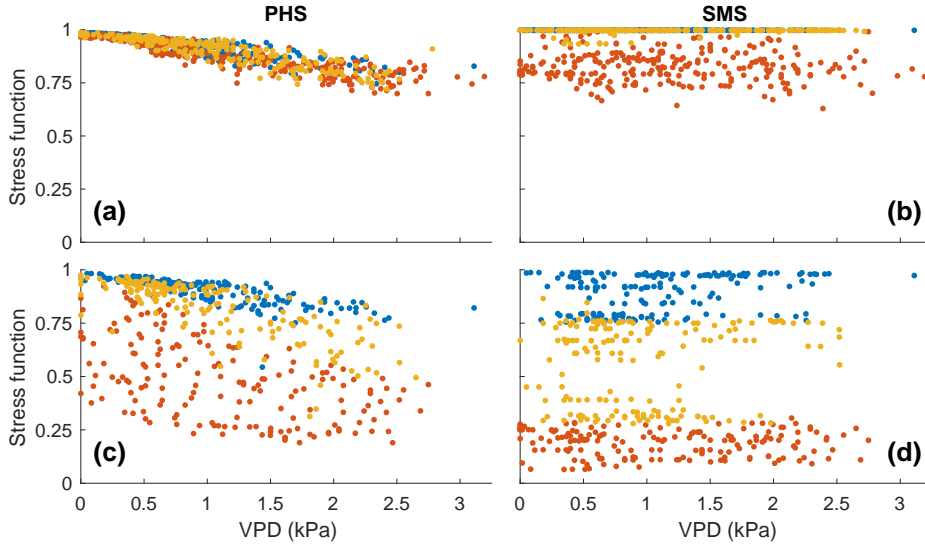
Figure 2. Modeled vegetation water potential at Caxiuanã, Brazil. (a) 2003 Dry season (SON) diurnal mean, ambient through-fall conditions, (b) 2003 Dry season (SON) diurnal mean, with 60% through-fall excluded. Curves are drawn for sunlit leaf, shaded leaf, stem, and root water potentials. Note that the first three mostly overlap. (c) Monthly mean midday leaf water potential, under ambient (solid line) and 60% through-fall exclusion (dotted line) conditions. Note that through-fall exclusion begins in month 11 (Nov 1, 2001).



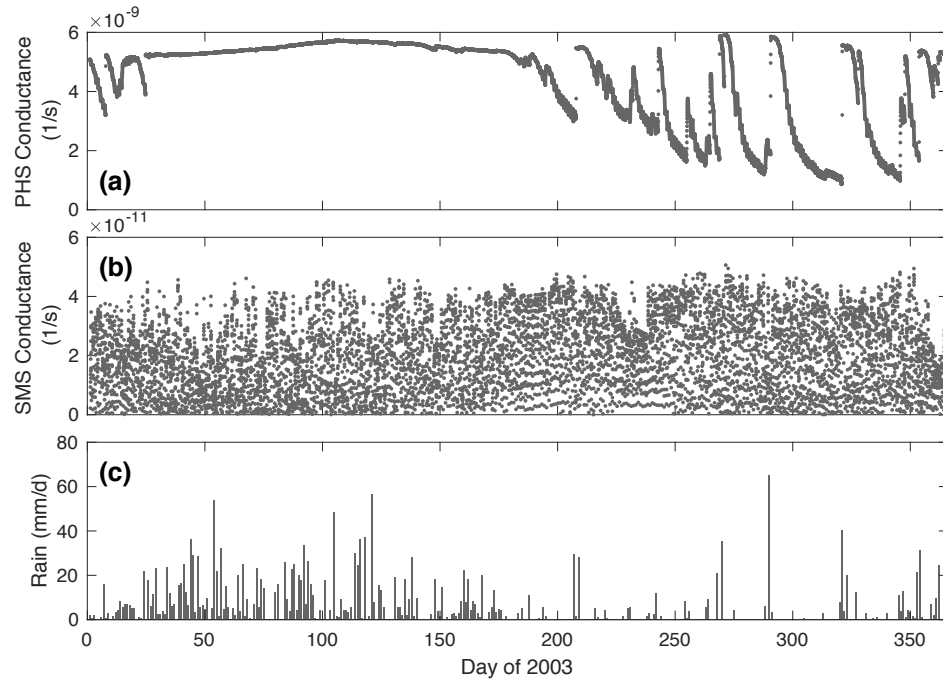
842 **Figure 3.** (a,b) Monthly mean water stress function. Note that the water stress function equals 1 when
 843 there is no stress and 0 when fully stressed. (c,d) Monthly mean transpiration (W/m^2). (e,f) Monthly mean
 844 gross primary productivity ($\text{g}/\text{m}^2/\text{d}$). Solid lines correspond to ambient through-fall conditions, and dotted
 845 lines feature 60% through-fall exclusion. Black lines represent model output. Red lines show observational
 846 transpiration derived from sap flux (see zqz). PHS is on for (a), (c), and (e). PHS is off for (b), (d), and (f).



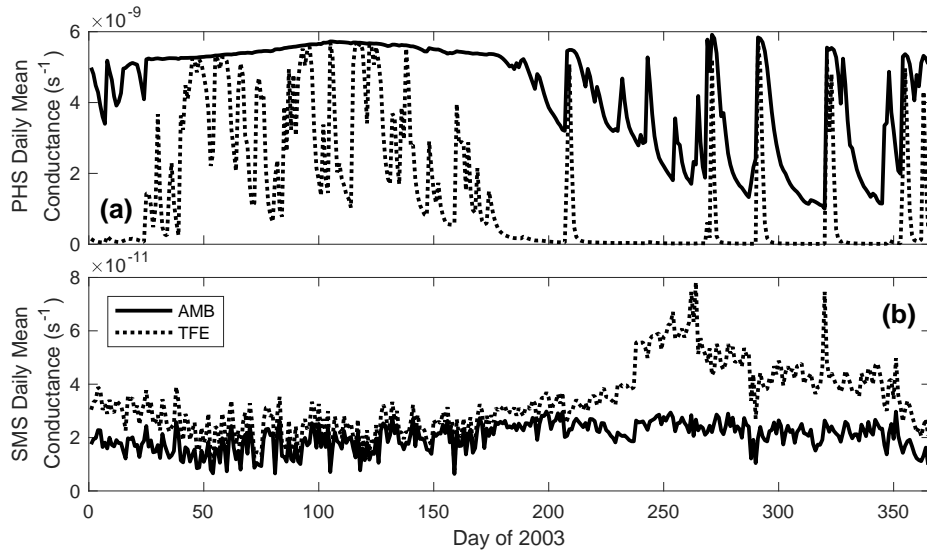
847 **Figure 4.** 2003 Dry season (SON) diurnal mean water stress function for (a) PHS on, and (b) PHS off.
848 Solid lines correspond to ambient through-fall conditions, and dotted lines feature 60% through-fall exclusion.
849 Note that the water stress function equals 1 when there is no stress and 0 when fully stressed.



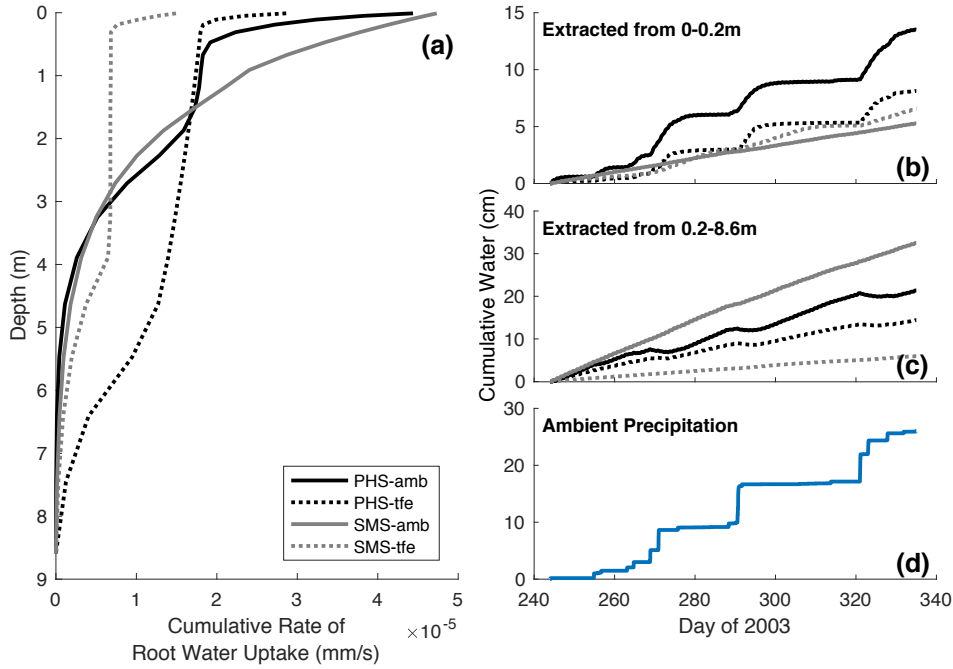
850 **Figure 5.** Water stress function versus vapor pressure deficit, for points with downwelling shortwave radia-
 851 tion between 400 and 425 W/m². (a) PHS, ambient through-fall (b) SMS, ambient through-fall (c) PHS,
 852 60% through-fall excluded (d) SMS, 60% through-fall excluded. For (a) and (c) data are subdivided based
 853 on predawn root water potential. For (b) and (d) data are subdivided based on average soil matric potential,
 854 weighted by root fraction. Blue dots represent the wettest tercile, yellow dots represent the intermediate ter-
 855 cile, and red dots represent the driest tercile. Note that panels (c) and (d) exclude data from 2001, when CO₂
 856 exclusion was not active.



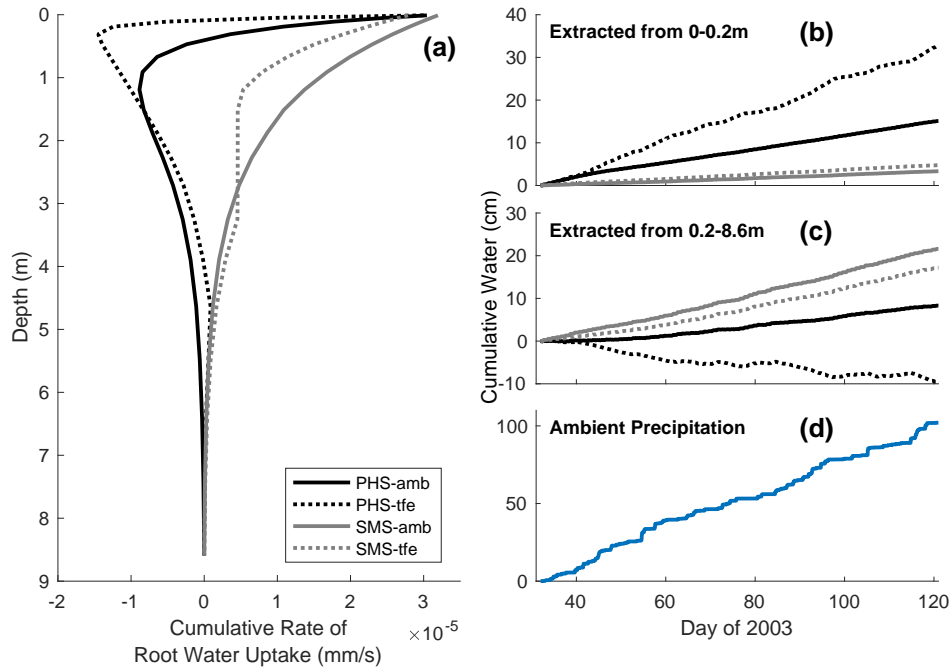
857 **Figure 6.** Soil Layer 3 conductance, under ambient through-fall conditions in 2003. (a) Time-series of
858 PHS modeled soil-to-root conductance (s^{-1}) from Soil Layer 3 (spanning 6 to 12 centimeters in depth). (b)
859 Time-series of SMS inferred conductance (s^{-1}) also from Soil Layer 3. (c) Concurrent precipitation forcing
860 (mm/d).



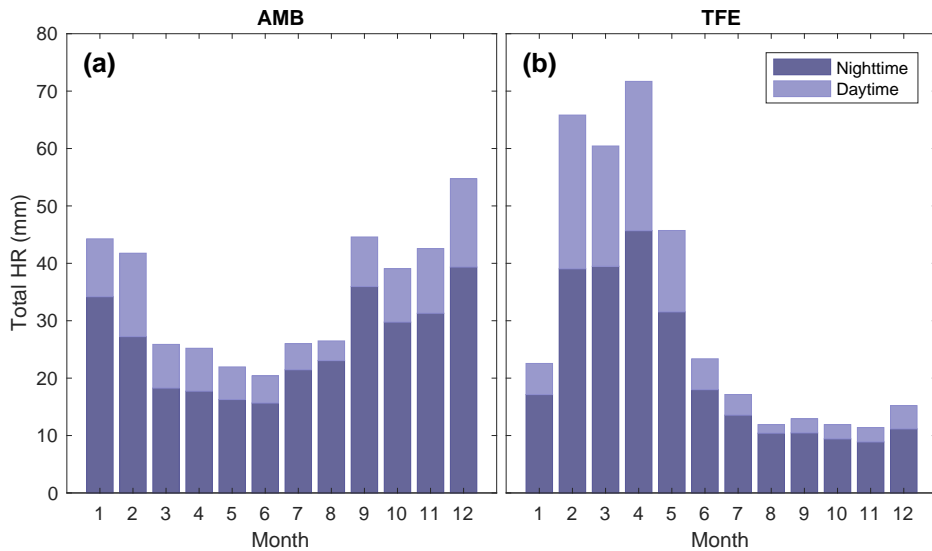
861 **Figure 7.** Daily mean Soil Layer 3 conductance, throughout 2003 under ambient (solid line) and 60%
862 through-fall exclusion (dotted line) conditions. (a) Daily mean of PHS modeled soil-to-root conductance (s^{-1})
863 from Soil Layer 3 (spanning 6 to 12 centimeters in depth). (b) Daily mean of SMS inferred conductance (s^{-1})
864 also from Soil Layer 3.



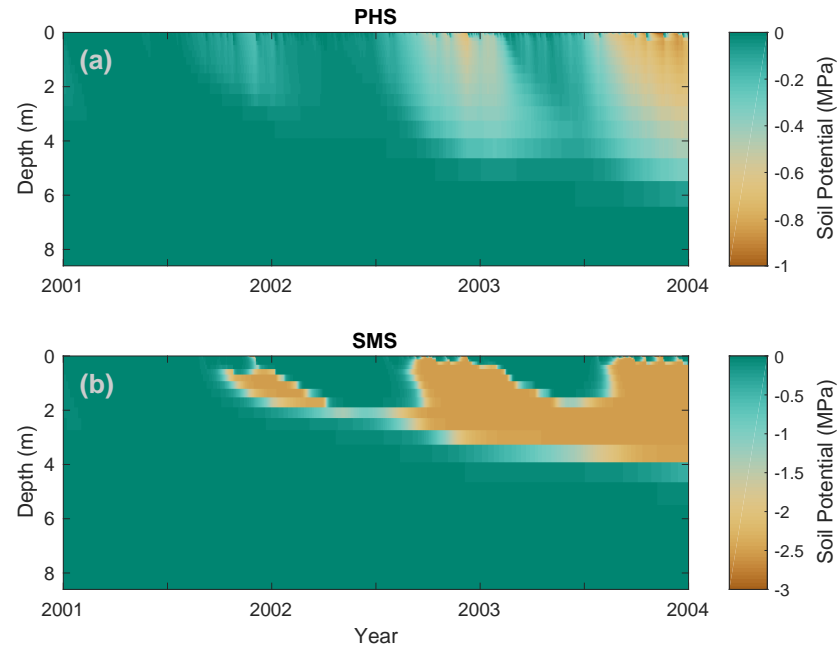
865 **Figure 8.** 2003 dry season (SON) root water uptake. Panel (a) shows the average cumulative profile of root
866 water uptake rate (mm/s) for the four simulations over SON-2003. Panel (b) shows cumulative total water
867 uptake from above 0.2m for the four simulations during SON-2003. Panel (c) shows cumulative total water
868 uptake from below 0.2m for the four simulations during SON-2003. Panel (d) shows cumulative total ambient
869 precipitation during SON-2003.



870 **Figure 9.** 2003 wet season (FMA) root water uptake. Panel (a) shows the average cumulative profile of root
871 water uptake rate (mm/s) for the four simulations over FMA-2003. Panel (b) shows cumulative total water
872 uptake from above 0.2m for the four simulations during FMA-2003. Panel (c) shows cumulative total water
873 uptake from below 0.2m for the four simulations during FMA-2003. Panel (d) shows cumulative total ambient
874 precipitation during FMA-2003.

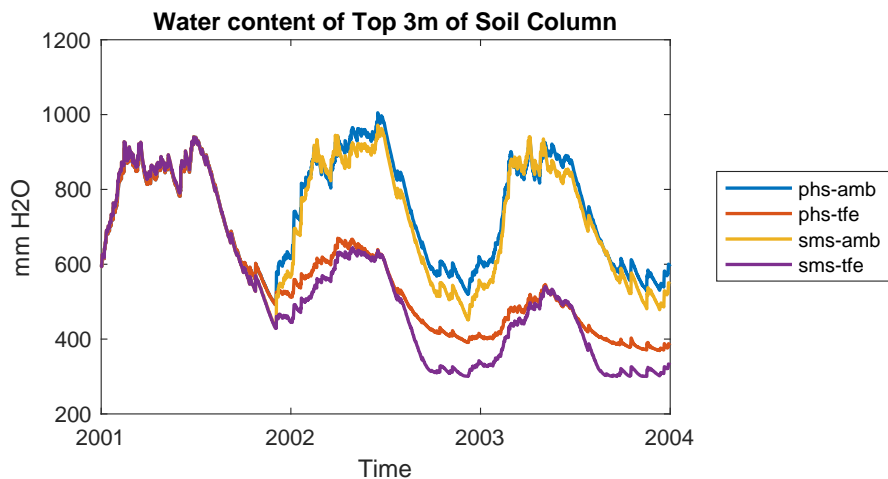


875 **Figure 10.** Total hydraulic redistribution (mm) by month in 2003. For (a) ambient through-fall conditions,
876 and (b) 60% through-fall exclusion. Darker shading shows portion of HR at night [6pm,6am], lighter shading
877 shows portion of HR during day [6am,6pm].

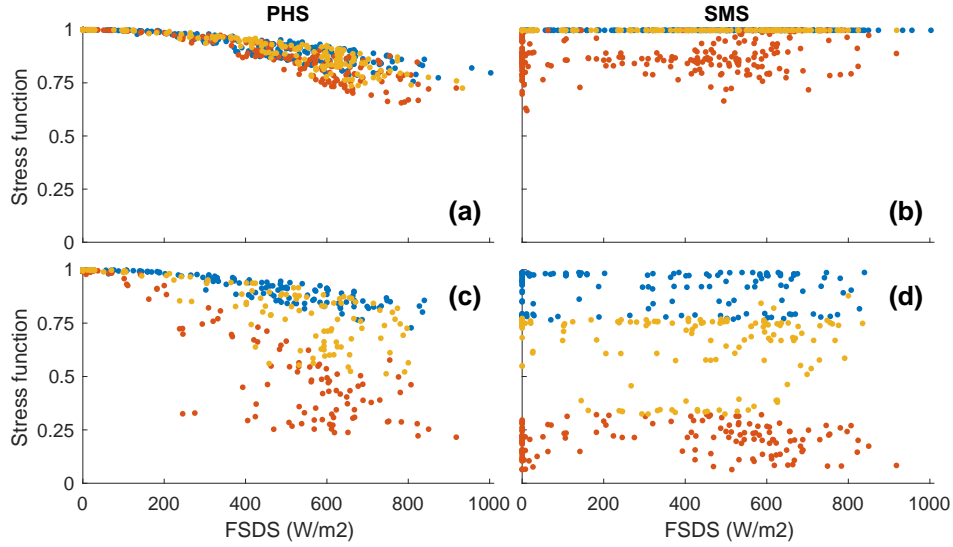


878 **Figure 11.** Vertical profile of soil water potential (MPa) over time under 60% through-fall exclusion, for (a)
879 PHS, and (b) SMS. Note that color axes are different.

880 **A: Supplementary Figures**



881 **Figure A.1.** Total water content of the top three meters of the soil column through time for the four simula-
882 tions.



883 **Figure A.2.** Water stress function versus downwelling shortwave radiation for points with vapor pressure
 884 deficit between 1 and 1.0559 kPa. (a) PHS, ambient through-fall (b) SMS, ambient through-fall (c) PHS,
 885 60% through-fall excluded (d) SMS, 60% through-fall excluded. For (a) and (c) data are subdivided based
 886 on predawn root water potential. For (b) and (d) data are subdivided based on average soil matric potential,
 887 weighted by root fraction. Blue dots represent the wettest tercile, yellow dots represent the intermediate
 888 tercile, and red dots represent the driest tercile. Note that panels (c) and (d) exclude data from 2001, when
 889 through-fall exclusion was not active.

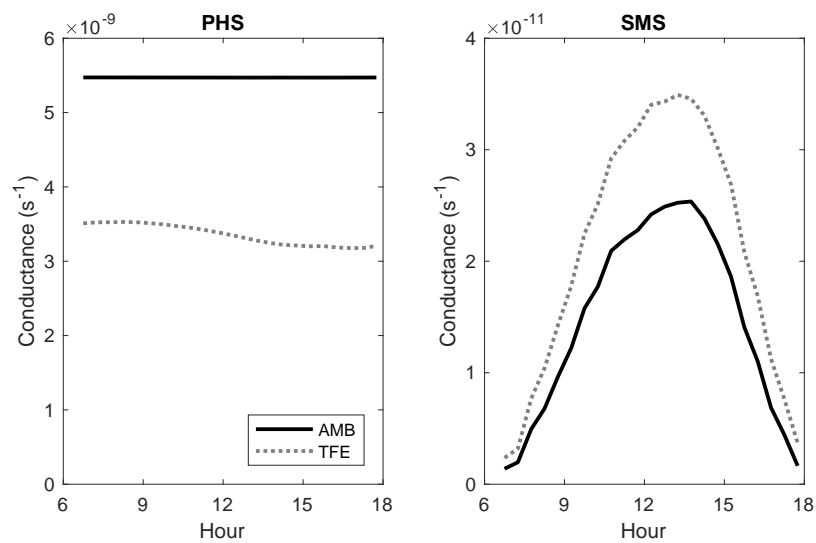


Figure A.3. FMA-2003 average diurnal cycle of layer 3 conductance.

890

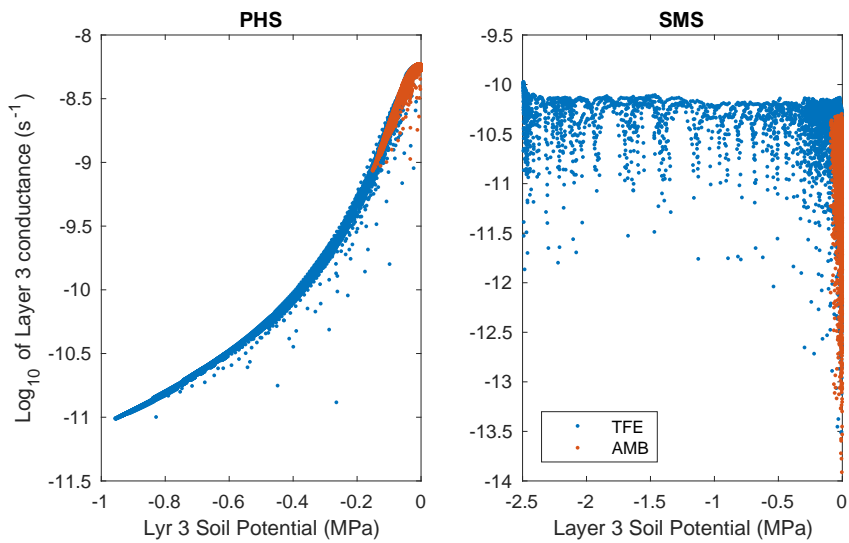


Figure A.4. Log of conductance versus soil potential for Soil Layer 3 (2003).

891

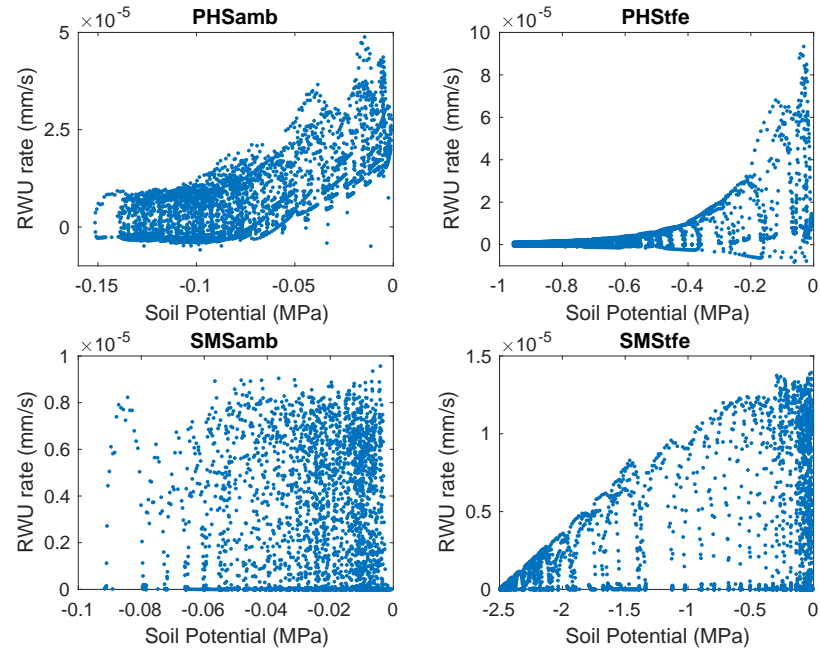
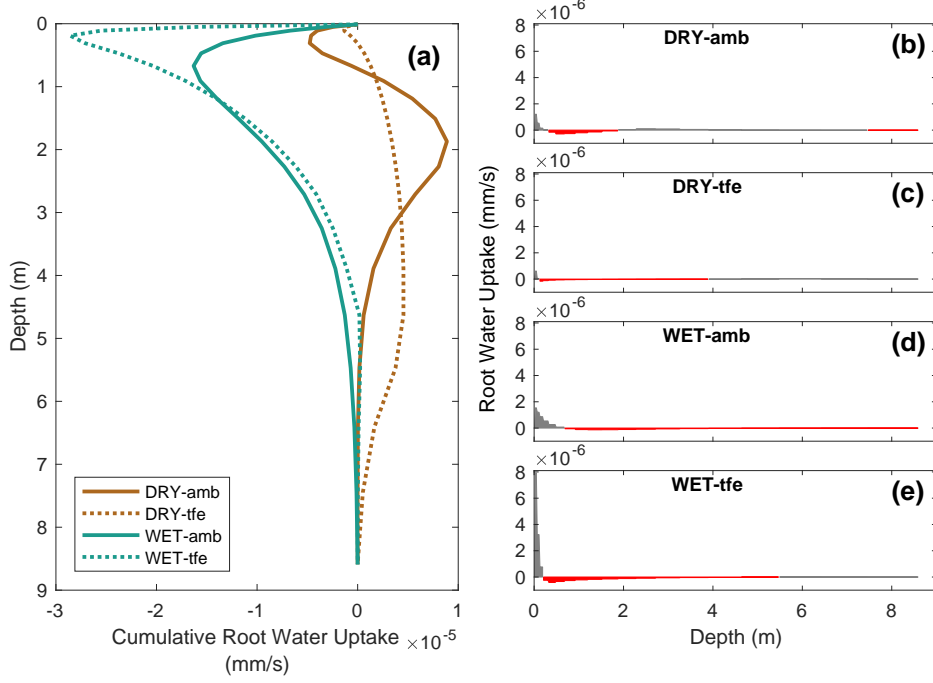
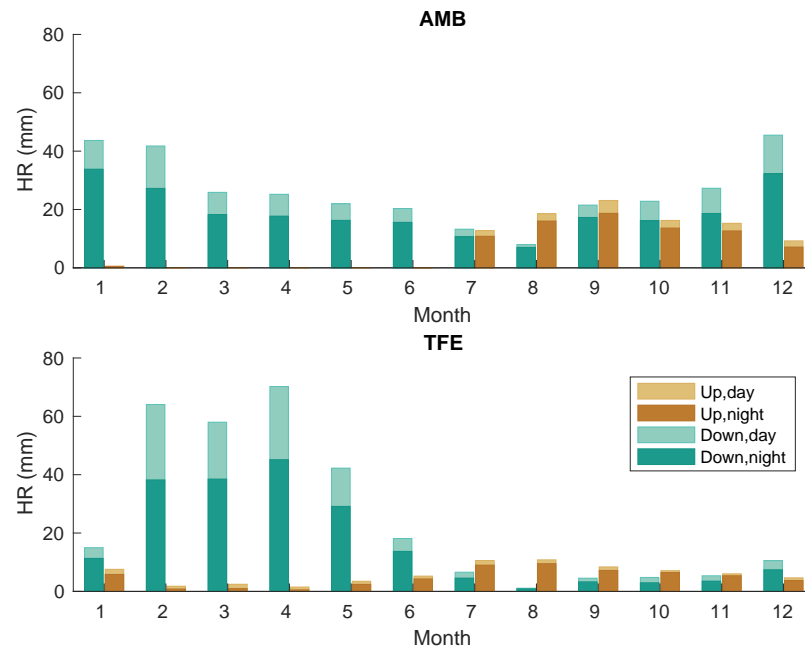


Figure A.5. Root water uptake versus soil potential for Soil Layer 3 (SON-2003).

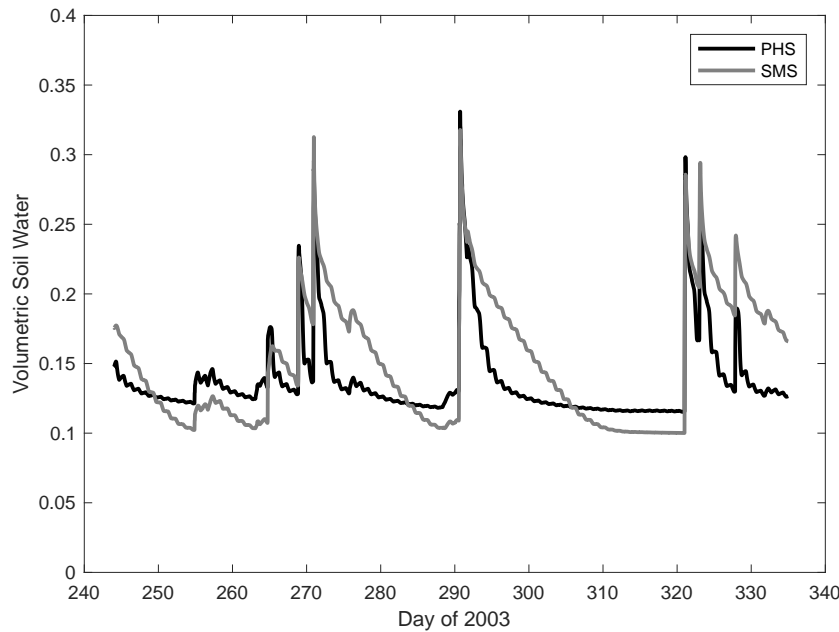
892



893 **Figure A.6.** PHS, nighttime (6pm to 6am) average root water uptake profiles with depth. Showing night-
 894 time serves to emphasize the profile of hydraulic redistribution. Panel (a) shows cumulative (starting at depth)
 895 root water uptake (mm/s) for ambient (solid line) and 60% through-fall exclusion (dotted line) during the wet
 896 (FMA, cyan color) and dry (SON, brown color) seasons. Panels (b)-(e) present the information from (a) in
 897 non-cumulative form. Note that for panels (b)-(e) negative root water uptake is shaded red, and also that for
 898 panel (a), positive slope indicates water uptake, and negative slope indicates water deposited. Note also that
 899 SMS is not shown, because hydraulic redistribution is precluded.



900 **Figure A.7.** PHS hydraulic distribution during 2003. Alternative version partitioning by direction.



901 **Figure A.8.** Volumetric soil water content in Soil Layer 2 (which spans 2-6cm in depth), for SON-2003,
902 featuring 60% through-fall exclusion. With PHS (black line), the soil layer can dry out much more quickly
903 after rain events.

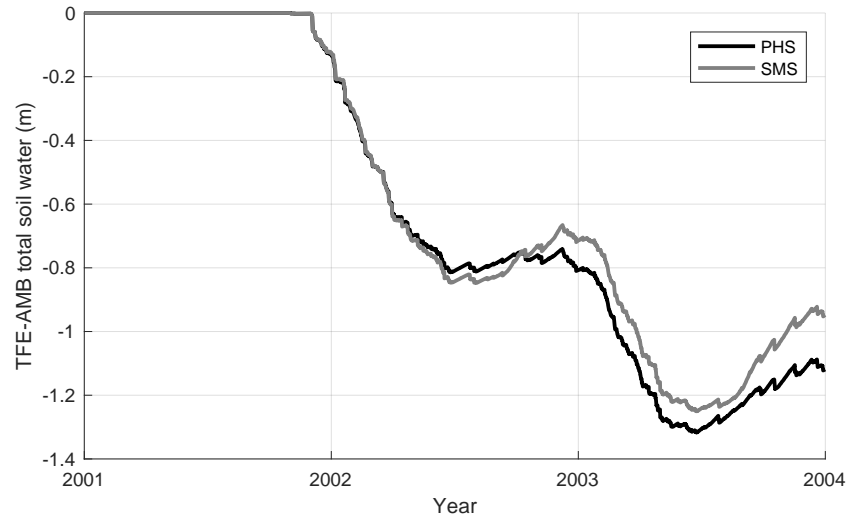
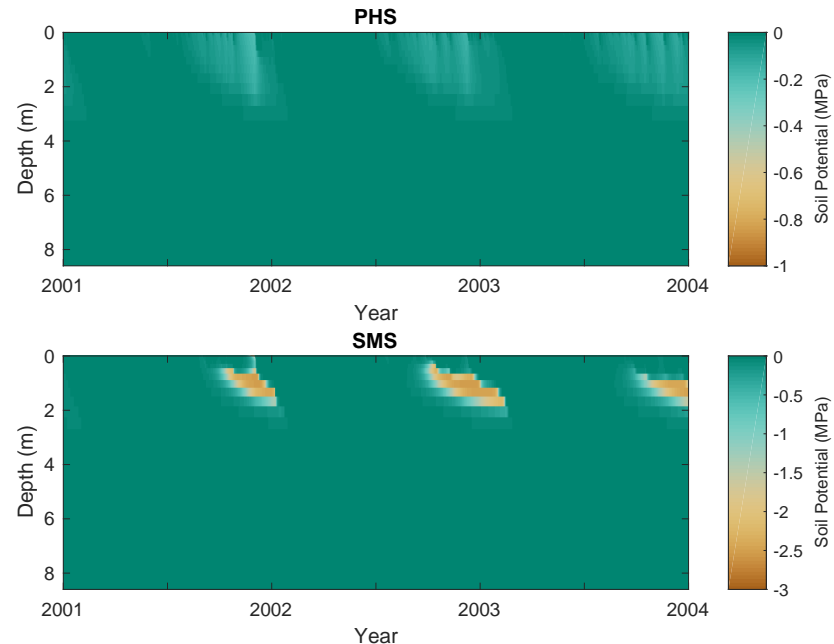
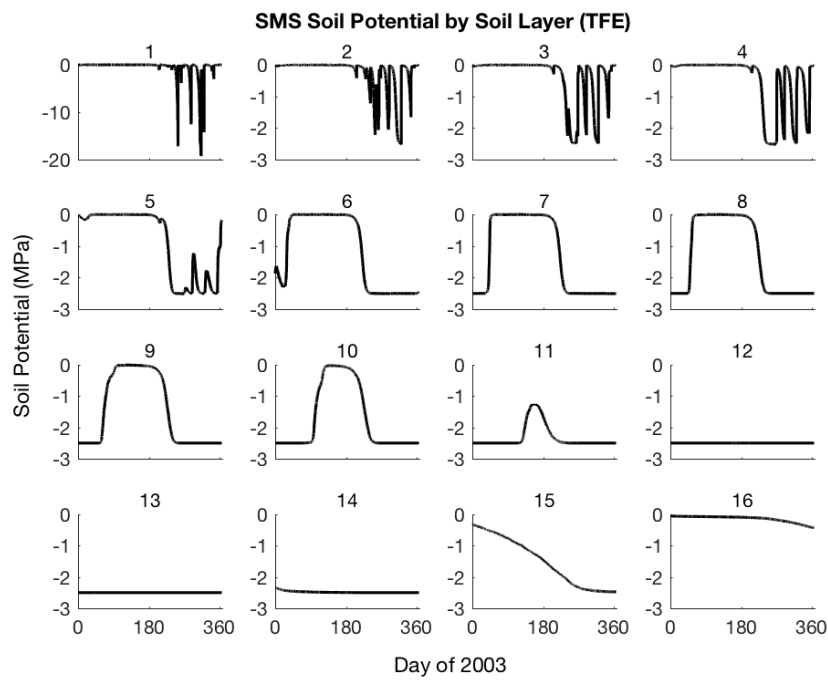


Figure A.9. Delta soil water

904



905 **Figure A.10.** Vertical profile of soil water potential (MPa) through time under ambient through-fall conditions,
906 for (a) PHS, and (b) SMS. Note that color axes are different.



907 **Figure A.11.** Time series of soil potential by soil layer, with SMS, under 60% through-fall exclusion. This
 908 duplicates the information in Figure 11a to highlight the the sensitivity of soil moisture dynamics to the SMS
 909 parameter, ψ_c (soil potential with stomates fully closed, -2.5 MPa). Soil Layers 17-20, which do not dry out
 910 completely (similar to Soil Layer 16), are not shown.

911 B: Appendix to Model Description

912 B.1 Details of Water Supply

913 PHS resolves flow across four different segments, soil-to-root, root-to-stem, stem-to-
 914 leaf, and leaf-to-transpiration.

915 Stem-to-leaf. The area bases are sunlit and shaded leaf area, respectively. Note that
 916 gravity is assumed negligible here. Likewise there is no length scaling applied to maximum
 917 conductance. Therefore the input parameters for $k_{1,\max}$ should be conductances (s^{-1}).

$$\begin{aligned} q_{1a} &= k_1 \cdot \text{LAI-sun} \cdot (\psi_{\text{stem}} - \psi_{\text{sun-leaf}}) \\ q_{1b} &= k_1 \cdot \text{LAI-shade} \cdot (\psi_{\text{stem}} - \psi_{\text{shade-leaf}}) \end{aligned} \quad (\text{B.1})$$

$$k_1 = k_{1,\max} \cdot f(\psi_{\text{stem}}) \quad (\text{B.2})$$

$$f(\psi) = 2^{-\left(\frac{\psi}{p_{50}}\right)^{c_k}} \quad (\text{B.3})$$

921 Root-to-stem. The area basis is stem area index. The parameter is maximum stem
 922 xylem conductivity ($K_{2,\max}$). Stem conductance (k_2) is the result of scaling maximum con-
 923 ductivity by the tree height (h) and applying loss relative to maximum conductance via the
 924 vulnerability curve $f(\psi_{\text{root}})$.

$$q_2 = k_2 \cdot \text{SAI} \cdot (\psi_{\text{root}} - \psi_{\text{stem}} - \rho g h) \quad (\text{B.4})$$

$$k_2 = \frac{K_{2,\max}}{h} \cdot f(\psi_{\text{root}}) \quad (\text{B.5})$$

925 Soil-to-root. Area basis is RAI in soil layer i , which is based on the layer root fraction
 926 times the total root area. Total root area we have as the summed stem and leaf area indices
 927 multiplied by a relative root area parameter (f_{root}). The vertical root distribution is defined
 928 by the layer root fraction (r_i), which follows a one-parameter (by PFT) power law decay fol-
 929 lowing Jackson *et al.* [1996].

$$q_{3,i} = k_{3,i} \cdot \text{RAI}_i \cdot (\psi_{\text{soil},i} - \psi_{\text{root}} - \rho g z_i) \quad (\text{B.6})$$

$$\text{RAI}_i = f_{\text{root}} \cdot (\text{SAI} + \text{LAI}) \cdot r_i \quad (\text{B.7})$$

$$k_{3,i} = \frac{k_{r,i} + k_{s,i}}{k_{r,i} \cdot k_{s,i}} \quad (\text{B.8})$$

$$k_{r,i} = \frac{K_{r,\max}}{l_i} f(\psi_{\text{soil},i}) \quad (\text{B.9})$$

$$l_i = z_i + x \quad (\text{B.10})$$

$$k_{s,i} = \frac{K_{s,i}}{d} \quad (\text{B.11})$$

944 The conductance $k_{3,i}$ reflects two resistors in series, from soil-to-root ($k_{s,i}$) and through
 945 the root tissue ($k_{r,i}$). The root tissue conductance is attenuated via the vulnerability curve
 946 framework. The input parameter is maximum root xylem conductivity, on the basis of RAI
 947 as defined above. The root conductivity is scaled by the conducting length, which is esti-
 948 mated as the sum of soil layer depth (z_i) and average lateral extent (x , static parameter). The
 949 soil conductivity $K_{s,i}$ is calculated from the layer soil matric potential (ψ_s) and soil proper-
 950 ties following Clapp and Hornberger [1978] as described in Oleson *et al.* [2013]. The soil
 951 conductance ($k_{s,i}$) is the result of scaling the conductivity by d , the distance between roots
 952 estimated following Williams *et al.* [1996] and Bonan *et al.* [2014]

953 The challenge here is obviously getting your head around all the parameters.

954 **B.2 Details of Water Demand**955 **B.3 Details of Solution**

956 The continuity of water flow through the system yields four equations

$$\begin{aligned} E_{sun} &= q_{1a} \\ E_{shade} &= q_{1b} \\ q_{1a} + q_{1b} &= q_2 \\ q_2 &= \sum_{i=1}^{nlevsoi} q_{3,i} \end{aligned} \quad (B.12)$$

958 We seek the set of vegetation water potential values (four unknowns),

$$\psi = \begin{bmatrix} \psi_{sunleaf} \\ \psi_{shadeleaf} \\ \psi_{stem} \\ \psi_{root} \end{bmatrix} \quad (B.13)$$

960 that satisfies these equations, as forced by the soil moisture and atmospheric state.

961 Each flux on the schematic can be represented in terms of the relevant water potentials.

962 Defining the transpiration fluxes:

$$\begin{aligned} E_{sun} &= E_{sun,max} \cdot 2^{-\left(\frac{\psi_{sunleaf}}{p50_e}\right)^{c_k}} \\ E_{shade} &= E_{shade,max} \cdot 2^{-\left(\frac{\psi_{shadeleaf}}{p50_e}\right)^{c_k}} \end{aligned} \quad (B.14)$$

964 Defining the water supply fluxes:

$$\begin{aligned} q_{1a} &= k_{1a,max} \cdot 2^{-\left(\frac{\psi_{stem}}{p50_1}\right)^{c_k}} \cdot LAI_{sun} \cdot (\psi_{stem} - \psi_{sunleaf}) \\ q_{1b} &= k_{1b,max} \cdot 2^{-\left(\frac{\psi_{stem}}{p50_1}\right)^{c_k}} \cdot LAI_{shade} \cdot (\psi_{stem} - \psi_{shadeleaf}) \\ q_2 &= \frac{k_{2,max}}{z_2} \cdot 2^{-\left(\frac{\psi_{root}}{p50_2}\right)^{c_k}} \cdot SAI \cdot (\psi_{root} - \psi_{stem} - \Delta\psi_z) \\ q_{soil} &= \sum_{i=1}^{nlevsoi} q_{3,i} = \sum_{i=1}^{nlevsoi} k_{3,i} \cdot RAI \cdot (\psi_{soil,i} - \psi_{root} + \Delta\psi_{z,i}) \end{aligned} \quad (B.15)$$

966 We're looking to find the vector ψ that fits with soil and atmospheric forcings while
967 satisfying water flow continuity. Due to the model non-linearity, we use a linearized explicit
968 approach, iterating with Newton's method. The initial guess is the solution for ψ (vector)
969 from the previous time step. The general framework, from iteration m to $m + 1$ is:

$$\begin{aligned} q^{m+1} &= q^m + \frac{\delta q}{\delta \psi} \Delta \psi \\ \psi^{m+1} &= \psi^m + \Delta \psi \end{aligned} \quad (B.16)$$

971 So for our first flux balance equation, at iteration $m + 1$, we have:

972

$$E_{sun}^{m+1} = q_{1a}^{m+1} \quad (\text{B.17})$$

973

Which can be linearized to:

974

$$E_{sun}^m + \frac{\delta E_{sun}}{\delta \psi} \Delta \psi = q_{1a}^m + \frac{\delta q_{1a}}{\delta \psi} \Delta \psi \quad (\text{B.18})$$

975

And rearranged to be:

976

$$\frac{\delta q_{1a}}{\delta \psi} \Delta \psi - \frac{\delta E_{sun}}{\delta \psi} \Delta \psi = E_{sun}^m - q_{1a}^m \quad (\text{B.19})$$

977

And for the other 3 flux balance equations:

978

$$\begin{aligned} \frac{\delta q_{1b}}{\delta \psi} \Delta \psi - \frac{\delta E_{sha}}{\delta \psi} \Delta \psi &= E_{sha}^m - q_{1b}^m \\ \frac{\delta q_2}{\delta \psi} \Delta \psi - \frac{\delta q_{1a}}{\delta \psi} \Delta \psi - \frac{\delta q_{1b}}{\delta \psi} \Delta \psi &= q_{1a}^m + q_{1b}^m - q_2^m \\ \frac{\delta q_{soil}}{\delta \psi} \Delta \psi - \frac{\delta q_2}{\delta \psi} \Delta \psi &= q_2^m - q_{soil}^m \end{aligned} \quad (\text{B.20})$$

979

Putting all four together in matrix form:

980

$$\begin{bmatrix} \frac{\delta q_{1a}}{\delta \psi} - \frac{\delta E_{sun}}{\delta \psi} \\ \frac{\delta q_{1b}}{\delta \psi} - \frac{\delta E_{sha}}{\delta \psi} \\ \frac{\delta q_2}{\delta \psi} - \frac{\delta q_{1a}}{\delta \psi} - \frac{\delta q_{1b}}{\delta \psi} \\ \frac{\delta q_{soil}}{\delta \psi} - \frac{\delta q_2}{\delta \psi} \end{bmatrix} \Delta \psi = \begin{bmatrix} E_{sun}^m - q_{1a}^m \\ E_{sha}^m - q_{1b}^m \\ q_{1a}^m + q_{1b}^m - q_2^m \\ q_2^m - q_{soil}^m \end{bmatrix} \quad (\text{B.21})$$

981

Now to expand the left-hand side, from vector ψ to the four distinct plant water potential nodes, noting that many derivatives are zero (e.g. $\frac{\delta E_{sun}}{\delta \psi_{sha}} = 0$)

982

Introducing the notation: $A \Delta \psi = b$

984

$$\Delta \psi = \begin{bmatrix} \Delta \psi_{sunleaf} \\ \Delta \psi_{shadeleaf} \\ \Delta \psi_{stem} \\ \Delta \psi_{root} \end{bmatrix} \quad (\text{B.22})$$

985

$$A = \begin{bmatrix} \frac{\delta q_{1a}}{\delta \psi_{sun}} - \frac{\delta E_{sun}}{\delta \psi_{sun}} & 0 & \frac{\delta q_{1a}}{\delta \psi_{stem}} & 0 \\ 0 & \frac{\delta q_{1b}}{\delta \psi_{sha}} - \frac{\delta E_{sha}}{\delta \psi_{sha}} & \frac{\delta q_{1b}}{\delta \psi_{stem}} & 0 \\ -\frac{\delta q_{1a}}{\delta \psi_{sun}} & -\frac{\delta q_{1b}}{\delta \psi_{sha}} & \frac{\delta q_2}{\delta \psi_{stem}} - \frac{\delta q_{1a}}{\delta \psi_{stem}} - \frac{\delta q_{1b}}{\delta \psi_{stem}} & \frac{\delta q_2}{\delta \psi_{root}} \\ 0 & 0 & -\frac{\delta q_2}{\delta \psi_{stem}} & \frac{\delta q_{soil}}{\delta \psi_{root}} - \frac{\delta q_2}{\delta \psi_{root}} \end{bmatrix} \quad (\text{B.23})$$

$$b = \begin{bmatrix} E_{sun}^m - q_{b1}^m \\ E_{shade}^m - q_{b2}^m \\ q_{b1}^m + q_{b2}^m - q_{stem}^m \\ q_{stem}^m - q_{soil}^m \end{bmatrix} \quad (\text{B.24})$$

Now we compute all the entries for A and b based on the soil moisture and maximum transpiration forcings and can solve to find:

$$\Delta\psi = A^{-1}b \quad (\text{B.25})$$

$$\psi_{m+1} = \psi_m + \Delta\psi \quad (\text{B.26})$$

We iterate until $b \rightarrow 0$, signifying water flux balance through the system. The result is a final set of water potentials ($\psi_{root}, \psi_{xylem}, \psi_{shadeleaf}, \psi_{sunleaf}$) satisfying non-divergent water flux through the system. The magnitude of the water flux is driven by soil matric potential and unstressed ($\beta_t = 1$) transpiration.

We use the transpiration solution (corresponding to the final solution for ψ) to compute stomatal conductance. The stomatal conductance is then used to compute β_t .

$$\beta_{t,sun} = \frac{g_{s,sun}}{g_{s,sun,\beta_t=1}} \quad (\text{B.27})$$

$$\beta_{t,shade} = \frac{g_{s,shade}}{g_{s,shade,\beta_t=1}} \quad (\text{B.28})$$

The β_t values are used in the Photosynthesis module (see section 2.1) to apply water stress. The solution for ψ is saved as a new variable (vegetation water potential) and is indicative of plant water status. The soil-to-root fluxes ($q_{3,1}, q_{3,2}, \dots, q_{3,n}$) are used as the soil transpiration sink in the Richards' equation subsurface flow equations.

Furthermore several simplifications were made that decrease the numerical complexity. For the purposes of the PHS solution, soil potentials are assumed constant during each timestep. Plant tissue water storage (capacitance) is not represented, whereby the solution does not depend on the previous timestep and has no time derivatives.

Acknowledgments

= enter acknowledgments here =

Pierre: Text I removed While there are disagreements about soil moisture trends globally [Dai, 2013; Sheffield et al., 2012], Amazonia has experienced and a lengthening dry season [Fu et al., 2013] and faces projections of increasing frequency of extreme El Niño events [Cai et al., 2014]

References

- Allen, C. D., A. K. Macalady, H. Chenchouni, D. Bachelet, N. McDowell, M. Vennetier, T. Kitzberger, A. Rigling, D. D. Breshears, E. T. Hogg, P. Gonzalez, R. Fensham, Z. Zhang, J. Castro, N. Demidova, J.-H. Lim, G. Allard, S. W. Running, A. Semerci, and N. Cobb (2010), A global overview of drought and heat-induced tree mortality reveals emerging climate change risks for forests, *Forest Ecology and Management*, 259(4), 660 – 684, doi:<https://doi.org/10.1016/j.foreco.2009.09.001>.

- 1020 Anderegg, W. R. L. (2015a), Spatial and temporal variation in plant hydraulic traits and their
 1021 relevance for climate change impacts on vegetation, *New Phytologist*, 205(3), 1008–1014,
 1022 doi:10.1111/nph.12907.
- 1023 Anderegg, W. R. L., J. M. Kane, and L. D. L. Anderegg (2013a), Consequences of
 1024 widespread tree mortality triggered by drought and temperature stress, *Nature Climate
 1025 Change*, 3(1), 30–36.
- 1026 Anderegg, W. R. L., L. Plavcová, L. D. L. Anderegg, U. G. Hacke, J. A. Berry, and C. B.
 1027 Field (2013b), Drought's legacy: multiyear hydraulic deterioration underlies widespread
 1028 aspen forest die-off and portends increased future risk, *Global Change Biology*, 19(4),
 1029 1188–1196, doi:10.1111/gcb.12100.
- 1030 Anderegg, W. R. L., C. Schwalm, F. Biondi, J. J. Camarero, G. Koch, M. Litvak, K. Ogle,
 1031 J. D. Shaw, E. Shevliakova, A. P. Williams, A. Wolf, E. Ziacon, and S. Pacala (2015b), Per-
 1032 vasive drought legacies in forest ecosystems and their implications for carbon cycle mod-
 1033 els, *Science*, 349(6247), 528–532, doi:10.1126/science.aab1833.
- 1034 Bartlett, M. K., T. Klein, S. Jansen, B. Choat, and L. Sack (2016), The correlations and se-
 1035 quence of plant stomatal, hydraulic, and wilting responses to drought, *Proceedings of the
 1036 National Academy of Sciences*, 113(46), 13,098–13,103, doi:10.1073/pnas.1604088113.
- 1037 Bonan, G. B., P. J. Lawrence, K. W. Oleson, S. Levis, M. Jung, M. Reichstein, D. M.
 1038 Lawrence, and S. C. Swenson (2011), Improving canopy processes in the Commu-
 1039 nity Land Model version 4 (CLM4) using global flux fields empirically inferred from
 1040 FLUXNET data, *Journal of Geophysical Research*, 116, doi:10.1029/2010JG001593.
- 1041 Bonan, G. B., M. Williams, R. A. Fisher, and K. W. Oleson (2014), Modeling stomatal con-
 1042 ductance in the earth system: linking leaf water-use efficiency and water transport along
 1043 the soil-plant-atmosphere continuum, *Geoscientific Model Development*, 7(5), 2193–2222,
 1044 doi:10.5194/gmd-7-2193-2014.
- 1045 Brooks, J. R., F. C. Meinzer, J. M. Warren, J.-C. Domec, and R. Coulombe (2006), Hydraulic
 1046 redistribution in a douglas-fir forest: lessons from system manipulations, *Plant, Cell &
 1047 Environment*, 29(1), 138–150, doi:10.1111/j.1365-3040.2005.01409.x.
- 1048 Burgess, S. S. O., M. A. Adams, N. C. Turner, and C. K. Ong (1998), The redistribution of
 1049 soil water by tree root systems, *Oecologia*, 115(3), 306–311, doi:10.1007/s004420050521.
- 1050 Cai, W., S. Borlace, M. Lengaigne, P. Van Renssch, M. Collins, G. Vecchi, A. Timmermann,
 1051 A. Santoso, M. J. McPhaden, L. Wu, M. H. England, G. Wang, E. Guilyardi, and F.-f. Jin
 1052 (2014), Increasing frequency of extreme El Niño events due to greenhouse warming, *Na-
 1053 ture Climate Change*, 4(2), 111–116.
- 1054 Celia, M. A., E. T. Bouloutas, and R. L. Zarba (1990), A general mass-conservative numer-
 1055 ical solution for the unsaturated flow equation, *Water Resources Research*, 26(7), 1483–
 1056 1496, doi:10.1029/WR026i007p01483.
- 1057 Choat, B., S. Jansen, T. J. Brodribb, H. Cochard, S. Delzon, R. Bhaskar, S. J. Bucci, T. S.
 1058 Feild, S. M. Gleason, U. G. Hacke, A. L. Jacobsen, F. Lens, H. Maherli, J. Martínez-
 1059 Vilalta, S. Mayr, M. Mencuccini, P. J. Mitchell, A. Nardini, J. Pitermann, R. B. Pratt, J. S.
 1060 Sperry, M. Westoby, I. J. Wright, and A. E. Zanne (2012), Global convergence in the vul-
 1061 nerability of forests to drought, *Nature*, 491(7426), 752–5.
- 1062 Christoffersen, B. O., M. Gloor, S. Fauset, N. M. Fyllas, D. R. Galbraith, T. R. Baker,
 1063 B. Kruijt, L. Rowland, R. A. Fisher, O. J. Binks, S. Sevanto, C. Xu, S. Jansen, B. Choat,
 1064 M. Mencuccini, N. G. McDowell, and P. Meir (2016), Linking hydraulic traits to tropi-
 1065 cal forest function in a size-structured and trait-driven model (tsfs v.1-hydro), *Geoscientific
 1066 Model Development*, 9(11), 4227–4255, doi:10.5194/gmd-9-4227-2016.
- 1067 Clapp, R. B., and G. M. Hornberger (1978), Empirical equations for some soil hydraulic
 1068 properties, *Water Resources Research*, 14(4), 601–604, doi:10.1029/WR014i004p00601.
- 1069 Collatz, G., J. Ball, C. Grivet, and J. A. Berry (1991), Physiological and environmental reg-
 1070 ulation of stomatal conductance, photosynthesis and transpiration: a model that includes
 1071 a laminar boundary layer, *Agricultural and Forest Meteorology*, 54(2), 107 – 136, doi:
 1072 http://dx.doi.org/10.1016/0168-1923(91)90002-8.

- da Costa, A. C., D. B. Metcalfe, C. E. Doughty, A. A. de Oliveira, G. F. Neto, M. C. da Costa, J. de Athaydes Silva Junior, L. E. Aragão, S. Almeida, D. R. Galbraith, L. M. Rowland, P. Meir, and Y. Malhi (2014), Ecosystem respiration and net primary productivity after 8–10 years of experimental through-fall reduction in an eastern Amazon forest, *Plant Ecology & Diversity*, 7(1–2), 7–24, doi:10.1080/17550874.2013.798366.
- da Costa, A. C. L., D. Galbraith, S. Almeida, B. Takeshi, T. Portela, M. da Costa, J. ao de Athaydes Silva Junior, A. P. Braga, P. H. L. de Gonçalves, A. A. de Oliveira, R. Fisher, O. L. Phillips, D. B. Metcalfe, P. Levy, and P. Meir (2010), Effect of 7 yr of experimental drought on vegetation dynamics and biomass storage of an eastern amazonian rainforest, *The New Phytologist*, 187(3), 579–591.
- Dai, A. (2013), Increasing drought under global warming in observations and models, *Nature Climate Change*, 3(1), 52–58.
- Dai, Y., R. E. Dickinson, and Y.-P. Wang (2004), A two-big-leaf model for canopy temperature, photosynthesis, and stomatal conductance, *Journal of Climate*, 17(12), 2281–2299, doi:10.1175/1520-0442(2004)017<2281:ATMFCT>2.0.CO;2.
- De Kauwe, M. G., J. Kala, Y.-S. Lin, A. J. Pitman, B. E. Medlyn, R. A. Duursma, G. Abramowitz, Y.-P. Wang, and D. G. Miralles (2015), A test of an optimal stomatal conductance scheme within the CABLE land surface model, *Geoscientific Model Development*, 8(2), 431–452, doi:10.5194/gmd-8-431-2015.
- De Kauwe, M. G., B. E. Medlyn, J. Knauer, and C. A. Williams (2017), Ideas and perspectives: how coupled is the vegetation to the boundary layer?, *Biogeosciences*, 14(19), 4435–4453, doi:10.5194/bg-14-4435-2017.
- Domec, J.-C., J. S. King, A. Noormets, E. Treasure, M. J. Gavazzi, G. Sun, and S. G. McNulty (2010), Hydraulic redistribution of soil water by roots affects whole-stand evapotranspiration and net ecosystem carbon exchange, *The New Phytologist*, 187(1), 171–183, doi:10.1111/j.1469-8137.2010.03245.x.
- Drake, J., S. Power, R. Duursma, B. Medlyn, M. Aspinwall, B. Choat, D. Creek, D. Eamus, C. Maier, S. Pfautsch, R. Smith, M. Tjoelker, and D. Tissue (2017), Stomatal and non-stomatal limitations of photosynthesis for four tree species under drought: A comparison of model formulations, *Agricultural and Forest Meteorology*, 247, 454 – 466, doi: <https://doi.org/10.1016/j.agrformet.2017.08.026>.
- Egea, G., A. Verhoef, and P. L. Vidale (2011), Towards an improved and more flexible representation of water stress in coupled photosynthesis-stomatal conductance models, *Agricultural and Forest Meteorology*, 151(10), 1370 – 1384, doi: <https://doi.org/10.1016/j.agrformet.2011.05.019>.
- Entekhabi, D., E. G. Njoku, P. E. O'Neill, K. H. Kellogg, W. T. Crow, W. N. Edelstein, J. K. Entin, S. D. Goodman, T. J. Jackson, J. Johnson, J. Kimball, J. R. Piepmeier, R. D. Koster, N. Martin, K. C. McDonald, M. Moghaddam, S. Moran, R. Reichle, J. C. Shi, M. W. Spencer, S. W. Thurman, L. Tsang, and J. V. Zyl (2010), The soil moisture active passive (smap) mission, *Proceedings of the IEEE*, 98(5), 704–716, doi: 10.1109/JPROC.2010.2043918.
- Epila, J., N. J. De Baerdemaeker, L. L. Vergeynst, W. H. Maes, H. Beeckman, and K. Steppe (2017), Capacitive water release and internal leaf water relocation delay drought-induced cavitation in African *Maesopsis eminii*, *Tree Physiology*, 37(4), 481–490, doi: 10.1093/treephys/tpw128.
- Farquhar, G. D., S. von Caemmerer, and J. A. Berry (1980), A biochemical model of photosynthetic CO₂ assimilation in leaves of C₃ species, *Planta*, 149(1), 78–90, doi: 10.1007/BF00386231.
- Ficklin, D. L., and K. A. Novick (2017), Historic and projected changes in vapor pressure deficit suggest a continental-scale drying of the United States atmosphere, *Journal of Geophysical Research: Atmospheres*, 122(4), 2061–2079, doi:10.1002/2016JD025855.
- Fisher, R. A., M. Williams, R. L. Do Vale, A. L. Da Costa, and P. Meir (2006), Evidence from Amazonian forests is consistent with isohydric control of leaf water potential, *Plant, Cell & Environment*, 29(2), 151–165, doi:10.1111/j.1365-3040.2005.01407.x.

- Fisher, R. A., M. Williams, A. L. D. Costa, Y. Malhi, R. F. D. Costa, S. Almeida, and P. Meir (2007), The response of an Eastern Amazonian rain forest to drought stress: results and modelling analyses from a throughfall exclusion experiment, *Global Change Biology*, 13(11), 2361–2378, doi:10.1111/j.1365-2486.2007.01417.x.
- Fisher, R. A., M. Williams, M. de Lourdes Ruivo, A. L. de Costa, and P. Meir (2008), Evaluating climatic and soil water controls on evapotranspiration at two Amazonian rainforest sites, *Agricultural and Forest Meteorology*, 148(6), 850 – 861, doi: <https://doi.org/10.1016/j.agrformet.2007.12.001>.
- Flexas, J., J. Bota, F. Loreto, G. Cornic, and T. D. Sharkey (2004), Diffusive and metabolic limitations to photosynthesis under drought and salinity in c3 plants, *Plant Biology*, 6(3), 269–279, doi:10.1055/s-2004-820867.
- Flexas, J., M. Ribas-Carbó, J. Bota, J. Galmés, M. Henkle, S. Martínez-Cañellas, and H. Medrano (2006), Decreased rubisco activity during water stress is not induced by decreased relative water content but related to conditions of low stomatal conductance and chloroplast CO₂ concentration, *New Phytologist*, 172(1), 73–82, doi:10.1111/j.1469-8137.2006.01794.x.
- Franks, P. J., P. L. Drake, and R. H. Froend (2007), Anisohydric but isohydrodynamic: seasonally constant plant water potential gradient explained by a stomatal control mechanism incorporating variable plant hydraulic conductance, *Plant, Cell & Environment*, 30(1), 19–30, doi:10.1111/j.1365-3040.2006.01600.x.
- Friedlingstein, P., M. Meinshausen, V. K. Arora, C. D. Jones, A. Anav, S. K. Liddicoat, and R. Knutti (2014), Uncertainties in CMIP5 climate projections due to carbon cycle feedbacks, *Journal of Climate*, 27(2), 511–526.
- Fu, R., L. Yin, W. Li, P. A. Arias, R. E. Dickinson, L. Huang, S. Chakraborty, K. Fernandes, B. Liebmann, R. Fisher, and R. B. Myneni (2013), Increased dry-season length over southern Amazonia in recent decades and its implication for future climate projection, *Proceedings of the National Academy of Sciences of the United States of America*, 110(45), 18,110–18,115.
- Gentine, P., M. Guérin, M. Uriarte, N. G. McDowell, and W. T. Pockman (2016), An allometry-based model of the survival strategies of hydraulic failure and carbon starvation, *Ecohydrology*, 9(3), 529–546, doi:10.1002/eco.1654.
- Grant, J., J.-P. Wigneron, R. D. Jeu, H. Lawrence, A. Mialon, P. Richaume, A. A. Bitar, M. Drusch, M. van Marle, and Y. Kerr (2016), Comparison of SMOS and AMSR-E vegetation optical depth to four MODIS-based vegetation indices, *Remote Sensing of Environment*, 172, 87 – 100, doi:<https://doi.org/10.1016/j.rse.2015.10.021>.
- Green, J. K., A. G. Konings, S. H. Alemohammad, J. Berry, D. Entekhabi, J. Kolassa, J.-E. Lee, and P. Gentine (2017), Regionally strong feedbacks between the atmosphere and terrestrial biosphere, *Nature Geoscience*, 10(6), 410–414, doi:10.1038/ngeo2957.
- Harley, P. C., R. B. Thomas, J. F. Reynolds, and B. R. Strain (1992), Modelling photosynthesis of cotton grown in elevated co₂, *Plant Cell Environment*, 15(3), 271–282, doi: 10.1111/j.1365-3040.1992.tb00974.x.
- Holbrook, N. M., E. T. Ahrens, M. J. Burns, and M. A. Zwieniecki (2001), In vivo observation of cavitation and embolism repair using magnetic resonance imaging, *Plant Physiology*, 126(1), 27–31, doi:10.1104/pp.126.1.27.
- Jackson, R. B., J. Canadell, J. R. Ehleringer, H. A. Mooney, O. E. Sala, and E. D. Schulze (1996), A global analysis of root distributions for terrestrial biomes, *Oecologia*, 108(3), 389–411, doi:10.1007/BF00333714.
- Kattge, J., S. DÄÑAz, S. Lavorel, I. C. Prentice, P. Leadley, G. BÄÑNisch, E. Garnier, M. Westoby, P. B. Reich, I. J. Wright, J. H. C. Cornelissen, C. Violle, S. P. Harrison, P. M. Van Bodegom, M. ReichSTEIN, B. J. Enquist, N. A. Soudzilovskaya, D. D. Ackerly, M. Anand, O. Atkin, M. Bahn, T. R. Baker, D. Baldocchi, R. Bekker, C. C. Blanco, B. Blonder, W. J. Bond, R. Bradstock, D. E. Bunker, F. Casanoves, J. Cavender-Bares, J. Q. Chambers, F. S. Chapin III, J. Chave, D. Coomes, W. K. Cornwell, J. M. Craine, B. H. Dobrin, L. Duarte, W. Durka, J. Elser, G. Esser, M. Estiarte, W. F. Fa-

- 1181 gan, J. Fang, F. Fernández-Mañdez, A. Fidelis, B. Finegan, O. Flores, H. Ford,
 1182 D. Frank, G. T. Freschet, N. M. Fyllas, R. V. Gallagher, W. A. Green, A. G. Gutierrez,
 1183 T. Hickler, S. I. Higgins, J. G. Hodgson, A. Jalili, S. Jansen, C. A. Joly, A. J. Kerkhoff,
 1184 D. Kirkup, K. Kitajima, M. Kleyer, S. Klotz, J. M. H. Knops, K. Kramer, I. Käijhn,
 1185 H. Kurokawa, D. Laughlin, T. D. Lee, M. Leishman, F. Lens, T. Lenz, S. L. Lewis,
 1186 J. Lloyd, J. Llusiá, F. Louault, S. Ma, M. D. MaHECHA, P. MaNNING, T. MaSSAD,
 1187 B. E. Medlyn, J. Messier, A. T. Moles, S. C. Mäijller, K. Nadrowski, S. Naeem, Á. Ni-
 1188 ninemets, S. Náúller, A. Nájjske, R. Ogaya, J. Oleksyn, V. G. Onipchenko, Y. Onoda,
 1189 J. Ordoñez, G. Overbeck, W. A. Ozinga, S. Patiño, S. Paula, J. G. Pausas, J. Peñuelas,
 1190 O. L. Phillips, V. Pillar, H. Poorter, L. Poorter, P. Poschlod, A. Prinzing, R. Proulx,
 1191 A. Rammig, S. Reinsch, B. Reu, L. Sack, B. Salgado-Negret, J. Sardans, S. Shiodera,
 1192 B. Shipley, A. Siefert, E. Sosinski, J.-F. Soussana, E. Swaine, N. Swenson, K. Thompson,
 1193 P. Thornton, M. Waldram, E. Weiher, M. White, S. White, S. J. Wright, B. Yguel, S. Za-
 1194 ehle, A. E. Zanne, and C. Wirth (2011), Try a global database of plant traits, *Global
 1195 Change Biology*, 17(9), 2905–2935, doi:10.1111/j.1365-2486.2011.02451.x.
- 1196 Klein, T., and S. Niu (2014), The variability of stomatal sensitivity to leaf water potential
 1197 across tree species indicates a continuum between isohydric and anisohydric behaviours,
 1198 *Functional Ecology*, 28(6), 1313–1320, doi:10.1111/1365-2435.12289.
- 1199 Konings, A. G., and P. Gentine (2017a), Global variations in ecosystem-scale isohydricity,
 1200 *Global Change Biology*, 23(2), 891–905, doi:10.1111/gcb.13389.
- 1201 Konings, A. G., M. Piles, K. Raützer, K. A. McColl, S. K. Chan, and D. Entekhabi (2016),
 1202 Vegetation optical depth and scattering albedo retrieval using time series of dual-polarized
 1203 l-band radiometer observations, *Remote Sensing of Environment*, 172, 178 – 189, doi:
 1204 https://doi.org/10.1016/j.rse.2015.11.009.
- 1205 Konings, A. G., A. P. Williams, and P. Gentine (2017b), Sensitivity of grassland productivity
 1206 to aridity controlled by stomatal and xylem regulation, *Nature Geoscience*, 10(4), 284–
 1207 288, doi:10.1038/ngeo2903.
- 1208 Lee, J.-E., R. S. Oliveira, T. E. Dawson, and I. Fung (2005), Root functioning modifies sea-
 1209 sonal climate, *Proceedings of the National Academy of Sciences of the United States of
 1210 America*, 102(49), 17,576–17,581, doi:10.1073/pnas.0508785102.
- 1211 Lin, C., P. Gentine, Y. Huang, K. Guan, H. Kimm, and S. Zhou (2018), Diel ecosys-
 1212 tem conductance response to vapor pressure deficit is suboptimal and indepen-
 1213 dent of soil moisture, *Agricultural and Forest Meteorology*, 250-251, 24 – 34, doi:
 1214 https://doi.org/10.1016/j.agrformet.2017.12.078.
- 1215 Mackay, D. S., D. E. Roberts, B. E. Ewers, J. S. Sperry, N. G. McDowell, and W. T. Pock-
 1216 man (2015), Interdependence of chronic hydraulic dysfunction and canopy processes can
 1217 improve integrated models of tree response to drought, *Water Resources Research*, 51(8),
 1218 6156–6176, doi:10.1002/2015WR017244.
- 1219 Manzoni, S., G. Vico, G. Katul, P. A. Fay, W. Polley, S. Palmroth, and A. Porporato (2011),
 1220 Optimizing stomatal conductance for maximum carbon gain under water stress: a meta-
 1221 analysis across plant functional types and climates, *Functional Ecology*, 25(3), 456–467,
 1222 doi:10.1111/j.1365-2435.2010.01822.x.
- 1223 Manzoni, S., G. Vico, S. Palmroth, A. Porporato, and G. Katul (2013a), Optimization of
 1224 stomatal conductance for maximum carbon gain under dynamic soil moisture, *Advances
 1225 in Water Resources*, 62, 90 – 105, doi:https://doi.org/10.1016/j.advwatres.2013.09.020.
- 1226 Manzoni, S., G. Vico, G. Katul, S. Palmroth, R. B. Jackson, and A. Porporato (2013b), Hy-
 1227draulic limits on maximum plant transpiration and the emergence of the safety-efficiency
 1228 trade-off, *New Phytologist*, 198(1), 169–178, doi:10.1111/nph.12126.
- 1229 McDowell, N. G., and C. D. Allen (2015), Darcy's law predicts widespread forest mortality
 1230 under climate warming, *Nature Climate Change*, 5(7), 669–672.
- 1231 McDowell, N. G., R. A. Fisher, C. Xu, J. C. Domec, T. Häußler, D. S. Mackay, J. S. Sperry,
 1232 A. Boutz, L. Dickman, N. Gehres, J. M. Limousin, A. Macalady, J. Martínez-Vilalta,
 1233 M. Mencuccini, J. A. Plaut, J. Ogale, R. E. Pangle, D. P. Rasse, M. G. Ryan, S. Sevanto,
 1234 R. H. Waring, A. P. Williams, E. A. Yepez, and W. T. Pockman (2013), Evaluating theo-

- ries of drought-induced vegetation mortality using a multimodel experiment framework, *New Phytologist*, 200(2), 304–321, doi:10.1111/nph.12465.
- McDowell, N. G., A. P. Williams, C. Xu, W. T. Pockman, L. T. Dickman, S. Sevanto, R. Pangle, J. Limousin, J. Plaut, D. S. Mackay, J. Ogee, J. C. Domec, C. D. Allen, R. A. Fisher, X. Jiang, J. D. Muss, D. D. Breshears, S. A. Rauscher, and C. Koven (2016), Multi-scale predictions of massive conifer mortality due to chronic temperature rise, *Nature Climate Change*, 6, 295–300, doi:10.1038/nclimate2873.
- Medlyn, B. E., R. A. Duursma, D. Eamus, D. S. Ellsworth, I. C. Prentice, C. V. M. Barton, K. Y. Crous, P. De Angelis, M. Freeman, and L. Wingate (2011), Reconciling the optimal and empirical approaches to modelling stomatal conductance, *Global Change Biology*, 17(6), 2134–2144, doi:10.1111/j.1365-2486.2010.02375.x.
- Meinzer, F. C., S. A. James, and G. Goldstein (2004), Dynamics of transpiration, sap flow and use of stored water in tropical forest canopy trees, *Tree Physiology*, 24(8), 901–909, doi:10.1093/treephys/24.8.901.
- Meinzer, F. C., D. M. Johnson, B. Lachenbruch, K. A. McCulloh, and D. R. Woodruff (2009), Xylem hydraulic safety margins in woody plants: coordination of stomatal control of xylem tension with hydraulic capacitance, *Functional Ecology*, 23(5), 922–930, doi:10.1111/j.1365-2435.2009.01577.x.
- Momen, M., J. D. Wood, K. A. Novick, R. Pangle, W. T. Pockman, N. G. McDowell, and A. G. Konings (2017), Interacting effects of leaf water potential and biomass on vegetation optical depth, *Journal of Geophysical Research: Biogeosciences*, 122(11), 3031–3046, doi:10.1002/2017JG004145.
- Nepstad, D. C., R. de Carvalho, Claudio, E. A. Davidson, P. H. Jipp, and e. al (1994), The role of deep roots in the hydrological and carbon cycles of amazonian forests and pastures, *Nature*, 372(6507), 666.
- Novick, K. A., D. L. Ficklin, P. C. Stoy, C. A. Williams, G. Bohrer, A. Oishi, S. A. Papuga, P. D. Blanken, A. Noormets, B. N. Sulman, R. L. Scott, L. Wang, and R. P. Phillips (2016a), The increasing importance of atmospheric demand for ecosystem water and carbon fluxes, *Nature Climate Change*, 6(11), 1023–1027.
- Novick, K. A., C. F. Miniat, and J. M. Vose (2016b), Drought limitations to leaf-level gas exchange: results from a model linking stomatal optimization and cohesion-tension theory, *Plant, Cell & Environment*, 39(3), 583–596, doi:10.1111/pce.12657.
- Oleson, K. W., D. M. Lawrence, G. B. Bonan, B. Drewniak, M. Huang, C. D. Koven, S. Levis, F. Li, W. J. Riley, Z. M. Subin, S. C. Swenson, P. E. Thornton, A. Bozbayik, R. Fisher, C. L. Heald, E. Kluzek, J.-F. Lamarque, P. J. Lawrence, L. R. Leung, W. Lipscomb, S. Muszala, D. M. Ricciuto, W. Sacks, Y. Sun, J. Tang, and Z.-L. Yang (2013), Technical description of version 4.5 of the community land model (clm), NCAR Tech. Note NCAR/TN-503+STR, *National Center for Atmospheric Research, Boulder, Colorado*, 420 pp., doi:10.5065/D6RR1W7M.
- Oliveira, R. S., T. E. Dawson, S. S. O. Burgess, and D. C. Nepstad (2005), Hydraulic redistribution in three amazonian trees, *Oecologia*, 145(3), 354–363, doi:10.1007/s00442-005-0108-2.
- Powell, T. L., D. R. Galbraith, B. O. Christoffersen, A. Harper, H. M. A. Imbuzeiro, L. Rowland, S. Almeida, P. M. Brando, A. C. L. da Costa, M. H. Costa, N. M. Levine, Y. Malhi, S. R. Saleska, E. Sotta, M. Williams, P. Meir, and P. R. Moorcroft (2013), Confronting model predictions of carbon fluxes with measurements of amazon forests subjected to experimental drought, *New Phytologist*, 200(2), 350–365, doi:10.1111/nph.12390.
- Restaino, C. M., D. L. Peterson, and J. Littell (2016), Increased water deficit decreases douglas fir growth throughout western US forests, *Proceedings of the National Academy of Sciences*, 113(34), 9557–9562, doi:10.1073/pnas.1602384113.
- Restrepo-Coupe, N., N. M. Levine, B. O. Christoffersen, L. P. Albert, J. Wu, M. H. Costa, D. Galbraith, H. Imbuzeiro, G. Martins, A. C. da Araujo, Y. S. Malhi, X. Zeng, P. Moorcroft, and S. R. Saleska (2017), Do dynamic global vegetation models capture the seasonality of carbon fluxes in the amazon basin? A data-model intercomparison, *Global Change*

- 1289 *Biology*, 23(1), 191–208, doi:10.1111/gcb.13442.
- 1290 Sack, L., P. J. Melcher, M. A. Zwieniecki, and N. M. Holbrook (2002), The hydraulic con-
1291 ductance of the angiosperm leaf lamina: a comparison of three measurement methods,
1292 *Journal of Experimental Botany*, 53(378), 2177–2184.
- 1293 Scholz, F. G., N. G. Phillips, S. J. Bucci, F. C. Meinzer, and G. Goldstein (2011), Hydraulic
1294 capacitance: Biophysics and functional significance of internal water sources, in Meinzer,
1295 F.C., Lachenbruch, B., Dawson, T. E. (eds) *Size- and Age-Related Changes in Tree Struc-*
1296 *ture and Function*, pp. 341–361, Springer, Dordrecht.
- 1297 Seager, R., A. Hooks, A. P. Williams, B. Cook, J. Nakamura, and N. Henderson (2015), Cli-
1298 matology, variability, and trends in the u.s. vapor pressure deficit, an important fire-related
1299 meteorological quantity, *Journal of Applied Meteorology and Climatology*, 54(6), 1121–
1300 1141, doi:10.1175/JAMC-D-14-0321.1.
- 1301 Sellers, P. J., D. A. Randall, G. J. Collatz, J. A. Berry, C. B. Field, D. A. Dazlich, C. Zhang,
1302 G. D. Collelo, and L. Bounoua (1996a), a revised land surface parameterization (sib2)
1303 for atmospheric gcms. part i: Model formulation, *Journal of Climate*, 9(4), 676–705, doi:
1304 10.1175/1520-0442(1996)009<0676:ARLSPF>2.0.CO;2.
- 1305 Sellers, P. J., C. J. Tucker, G. J. Collatz, S. O. Los, C. O. Justice, D. A. Dazlich, and
1306 D. A. Randall (1996b), A revised land surface parameterization (sib2) for atmo-
1307 spheric gcms. part ii: The generation of global fields of terrestrial biophysical pa-
1308 rameters from satellite data, *Journal of Climate*, 9(4), 706–737, doi:10.1175/1520-
1309 0442(1996)009<0706:ARLSPF>2.0.CO;2.
- 1310 Sheffield, J., E. F. Wood, and M. L. Roderick (2012), Little change in global drought over the
1311 past 60 years, *Nature*, 491(7424), 435–8.
- 1312 Simonin, K. A., E. Burns, B. Choat, M. M. Barbour, T. E. Dawson, and P. J. Franks (2015),
1313 Increasing leaf hydraulic conductance with transpiration rate minimizes the water potential
1314 drawdown from stem to leaf, *Journal of Experimental Botany*, 66(5), 1303–1315, doi:
1315 10.1093/jxb/eru481.
- 1316 Siqueira, M., G. Katul, and A. Porporato (2008), Onset of water stress, hysteresis in plant
1317 conductance, and hydraulic lift: Scaling soil water dynamics from millimeters to meters,
1318 *Water Resources Research*, 44(1), W01,432, doi:10.1029/2007WR006094.
- 1319 Sperry, J. S., and D. M. Love (2015), What plant hydraulics can tell us about responses to
1320 climate-change droughts, *New Phytologist*, 207(1), 14–27, doi:10.1111/nph.13354.
- 1321 Sperry, J. S., F. R. Adler, G. S. Campbell, and J. P. Comstock (1998), Limitation of plant
1322 water use by rhizosphere and xylem conductance: results from a model, *Plant Cell Envi-*
1323 *ronment*, 21(4), 347–359, doi:10.1046/j.1365-3040.1998.00287.x.
- 1324 Sperry, J. S., U. G. Hacke, R. Oren, and J. P. Comstock (2002), Water deficits and hy-
1325 draulic limits to leaf water supply, *Plant, Cell & Environment*, 25(2), 251–263, doi:
1326 10.1046/j.0016-8025.2001.00799.x.
- 1327 Sperry, J. S., M. D. Venturas, W. R. L. Anderegg, M. Mencuccini, D. S. Mackay, Y. Wang,
1328 and D. M. Love (2017), Predicting stomatal responses to the environment from the op-
1329 timization of photosynthetic gain and hydraulic cost, *Plant, Cell & Environment*, 40(6),
1330 816–830, doi:10.1111/pce.12852, pCE-16-0541.R1.
- 1331 Thornton, P. E., and N. E. Zimmermann (2007), An improved canopy integration scheme for
1332 a land surface model with prognostic canopy structure, *Journal of Climate*, 20(15), 3902–
1333 3923, doi:10.1175/JCLI4222.1.
- 1334 Tyree, M. T., and J. S. Sperry (1988), Do woody plants operate near the point of catastrophic
1335 xylem dysfunction caused by dynamic water stress?: Answers from a model, *Plant Physi-
1336 ology*, 88(3), 574–580.
- 1337 Tyree, M. T., and J. S. Sperry (1989), Vulnerability of xylem to cavitation and embolism,
1338 *Annual Review of Plant Physiology and Plant Molecular Biology*, 40(1), 19–36, doi:
1339 10.1146/annurev.pp.40.060189.000315.
- 1340 Ukkola, A. M., M. G. D. Kauwe, A. J. Pitman, M. J. Best, G. Abramowitz, V. Haverd,
1341 M. Decker, and N. Haughton (2016), Land surface models systematically overestimate the
1342 intensity, duration and magnitude of seasonal-scale evaporative droughts, *Environmental*

- 1343 *Research Letters*, 11(10), 104,012.
- 1344 Verhoef, A., and G. Egea (2014), Modeling plant transpiration under limited soil water:
- 1345 Comparison of different plant and soil hydraulic parameterizations and preliminary im-
- 1346 plications for their use in land surface models, *Agricultural and Forest Meteorology*, 191,
- 1347 22–32, doi:<https://doi.org/10.1016/j.agrformet.2014.02.009>.
- 1348 Williams, A. P., C. D. Allen, A. K. Macalady, D. Griffin, C. A. Woodhouse, D. M. Meko,
- 1349 T. W. Swetnam, S. A. Rauscher, R. Seager, H. Grissino-Mayer, J. S. Dean, E. R. Cook,
- 1350 C. Gangodagamage, M. Cai, and N. G. McDowell (2013), Temperature as a potent driver
- 1351 of regional forest drought stress and tree mortality, *Nature Climate Change*, 3(3), 292–297.
- 1352 Williams, M., E. B. Rastetter, D. N. Fernandes, M. L. Goulden, S. C. Wofsy, G. R. Shaver,
- 1353 J. M. Melillo, J. W. Munger, S.-M. Fan, and K. J. Nadelhoffer (1996), Modelling the soil-
- 1354 plant-atmosphere continuum in a *Quercus* stand at Harvard Forest: the regulation of
- 1355 stomatal conductance by light, nitrogen and soil/plant hydraulic properties, *Plant, Cell &*
- 1356 *Environment*, 19(8), 911–927, doi:[10.1111/j.1365-3040.1996.tb00456.x](https://doi.org/10.1111/j.1365-3040.1996.tb00456.x).
- 1357 Williams, M., B. E. Law, P. M. Anthoni, and M. H. Unsworth (2001), Use of a simulation
- 1358 model and ecosystem flux data to examine carbon–water interactions in ponderosa
- 1359 pine., *Tree Physiology*, 21(5), 287 – 298.
- 1360 Xu, X., D. Medvigy, J. S. Powers, J. M. Becknell, and K. Guan (2016), Diversity in plant
- 1361 hydraulic traits explains seasonal and inter-annual variations of vegetation dynamics in
- 1362 seasonally dry tropical forests, *New Phytologist*, 212(1), 80–95, doi:[10.1111/nph.14009](https://doi.org/10.1111/nph.14009),
- 1363 2015-20772.
- 1364 Zhou, S., R. A. Duursma, B. E. Medlyn, J. W. Kelly, and I. C. Prentice (2013), How should
- 1365 we model plant responses to drought? An analysis of stomatal and non-stomatal re-
- 1366 sponses to water stress, *Agricultural and Forest Meteorology*, 182-183, 204 – 214, doi:
- 1367 <https://doi.org/10.1016/j.agrformet.2013.05.009>.
- 1368 Zhou, S., B. Medlyn, S. Sabaté, D. Sperlich, I. C. Prentice, and D. Whitehead (2014), Short-
- 1369 term water stress impacts on stomatal, mesophyll and biochemical limitations to photosyn-
- 1370 thesis differ consistently among tree species from contrasting climates, *Tree Physiology*,
- 1371 34(10), 1035, doi:[10.1093/treephys/tpu072](https://doi.org/10.1093/treephys/tpu072).